Methane emissions are predominantly responsible for record-breaking atmospheric methane growth rates in 2020 and 2021

Liang Feng[1], Paul I. Palmer[1,2,*], Robert J. Parker[3,4], Mark F. Lunt[2], Hartmut Bösch[3,4]

1 National Centre for Earth Observation, University of Edinburgh, Edinburgh, UK

2 School of GeoSciences, University of Edinburgh, Edinburgh, UK

3 National Centre for Earth Observation, Space Park Leicester, University of Leicester, UK

4 Earth Observation Science, School of Physics and Astronomy, University of Leicester, UK

Correspondence to: Paul I. Palmer (paul.palmer@ed.ac.uk)

Abstract. The global atmospheric methane growth rates reported by NOAA for 2020 and 2021 are the largest since systematic measurements began in 1983. To explore the underlying reasons for these anomalous growth rates we use newly available methane data from the Japanese Greenhouse gases Observing SATellite (GOSAT) to estimate methane surface emissions. Relative to baseline values in 2019, we find a significant global increase in methane emission of 27.0±11.3 Tg and 20.8±11.4 Tg is needed to reproduce observed atmospheric methane in 2020 and 2021, respectively, assuming fixed climatological values for OH. We see the largest annual increases in methane emissions during 2020 over Eastern Africa (14±3 Tg), tropical Asia (3±4 Tg), tropical South America (5±4 Tg), and temperate Eurasia (3±3 Tg), and the largest reductions over China (-6±3 Tg) and India (-2±3 Tg). We find comparable emission changes in 2021, relative to 2019, except for tropical and temperate South America where emissions increased by 9±4 Tg and 4±3 Tg, respectively, and for temperate North America where emissions increased by 5±2 Tg. The elevated contributions we saw in 2020 over the western half of Africa (-5±3 Tg) are substantially reduced in 2021, compared to our 2019 baseline. We find statistically significant positive correlations between anomalies of tropical methane emissions and groundwater, consistent with recent studies that have highlighted a growing role for microbial sources over the tropics. Emission reductions over India and China are expected in 2020 due to the Covid-19 shutdown but continued in 2021, which we do not currently understand. To investigate the role of reduced OH concentrations during Covid-19 lockdowns in 2020 on the elevated atmospheric methane growth in 2020/2021, we extended our inversion state vector to include monthly scaling factors for OH concentrations over six latitude bands. During 2020, we find that tropospheric OH reduced by 1.4±1.7% relative to the corresponding 2019 baseline value. The corresponding revised global growth of *a posteriori* methane emissions in 2020 decreased by 34% to 17.9±13.2 Tg, relative to the *a posteriori* value that we inferred using fixed climatological OH values, consistent with sensitivity tests using the OH climatology inversion using reduced values for OH. The counter statement is that 66% of the global increase in atmospheric methane during 2020 was due to increased emissions, particularly from tropical regions. Regional flux differences between the joint methane-OH inversion and the OH climatology inversion in 2020 are typically much smaller than 10%. We find during 2021 that OH reduced by a much smaller

amount than in 2020, representing about 10% of the growth of atmospheric methane in that year. We conclude therefore that most of the observed increase in atmospheric methane during 2020 and 2021 is due to increased emissions, with a significant contribution from reduced levels of OH.

1 Introduction

The atmospheric growth rate of methane in the 21st century has defied a definitive explanation: following a period of near-zero growth during 2000-2007 (Rigby et al. 2008) growth rates have accelerated, with values reported by NOAA for 2020 (15.19±0.41 ppb) and 2021 (18.12±0.47 ppb) exceeding all prior values since their records began in 1983. The underlying reasons for these anomalous growth rates in 2020 and 2021 are currently subject to intense debate with some studies attributing most of the growth in 2020 to a reduction in the hydroxyl radical (OH) sink of methane due to global-scale reductions in nitrogen oxides due to pandemic-related industry shutdowns (Laughner et al. 2021). On the face of it, this appears to be a reasonable explanation, but recent studies have used satellite observations of atmospheric methane to reveal regional hotspots over the tropics that are responding to changes in climate and have global significance (Pandey et al. 2021; Lunt et al. 2019; 2021; Pandey et al. 2017; Feng, Palmer, Zhu, et al. 2022; Palmer et al. 2021; Wilson et al. 2020). Here, we use satellite observation of methane from the Japanese Greenhouse gases Observing SATellite (GOSAT) to document global and regional changes in emissions, extending a recent study (Feng, Palmer, Zhu, et al. 2022). In the next section we describe the data and methods used to infer methane emissions. In section 3 we describe our results and conclude the study in section 4.

2 Data and Methods

We follow closely the methodology from a recent study (Feng, Palmer, Zhu, et al. 2022) in which we simultaneously infer methane and CO_2 fluxes in 2020 and 2021 by directly assimilating proxy GOSAT XCH_4:XCO_2 retrievals (X denotes atmospheric column-averaged dry-air mole fraction). These data are anchored by surface methane and CO_2 measurements from an *in situ* observation network. The main advantage of this approach is that it does not rely on assumed model CO_2 concentrations to extract XCH_4 from the proxy ratio. For the sake of brevity, we include only details relevant to the calculations shown here.

2.1 GOSAT methane proxy data

We use version 9.0 of the proxy GOSAT XCH_4:XCO_2 retrievals from the University of Leicester (R. J. Parker et al. 2020; R. Parker and Boesch 2020), including both nadir observations over land and glint observations over the ocean. Analyses have shown that these retrievals have a bias of 0.2%, with a single-sounding precision of ~0.72%. We globally remove a slightly larger 0.3% bias from the GOSAT proxy data to improve the comparison with independent *in situ* observations (Feng et al. 2017; Feng, Palmer, Parker, et al. 2022). We assume that each single GOSAT proxy XCH_4:XCO_2 ratio retrieval has an

uncertainty of 1.2% to account for possible model errors, including the errors in atmospheric chemistry and transport, which helps to prevent model overfitting to observations.

2.2 *In situ* data

To anchor the GOSAT proxy ratio observations (Fraser et al. 2014b), we also ingest simultaneously the CO_2 and methane mole fraction data at surface-based sites, chosen from the NOAA compilation of the multi-laboratory *in-situ* measurements (Di Sarra et al. 2021; 2022; Cox et al. 2021; Cox, Di Sarra, Karion, et al. 2022). We include the same subset of the surface sites used by a recent study that documented year to year variations of methane emissions during 2010-2019 (Feng, Palmer, Zhu, et al. 2022). We assume uncertainties of 0.5 ppm and 8 ppb for these *in situ* observations of CO_2 and methane respectively (Feng, Palmer, Zhu, et al. 2022). We take advantage of the latest CO_2 (GLOBALVIEWplus v8.0 ObsPack) (Cox et al. 2021; Cox, Di Sarra, Vermeulen, et al. 2022) and methane (GLOBALVIEWplus v5.0 ObsPack) (Di Sarra et al. 2022; 2021) data products to study 2020 and 2021.

2.3 GEOS-Chem atmospheric chemistry transport model

We use the GEOS-Chem model of atmospheric chemistry and transport at a horizontal resolution of 2° (latitude) × 2.5° (longitude), driven by the MERRA2 meteorological reanalyses from the Global Modeling and Assimilation Office Global Circulation Model based at NASA Goddard Space Flight Center.

Our CO_2 and methane model calculations are described in a recent study (Feng, Palmer, Zhu, et al. 2022). The *a priori* CO_2 flux inventory includes monthly biomass burning emission (van der Werf et al. 2017); monthly fossil fuel emissions for 2019 in the absence of more recent data (Oda and Maksyutov 2021); monthly climatological ocean fluxes (Takahashi et al. 2009); and 3-hourly terrestrial biosphere fluxes (Randerson et al. 1996).

The *a priori* methane fluxes from nature include monthly wetland emissions, including rice paddies (Bloom et al. 2017); monthly fire methane emissions (van der Werf et al. 2017); and termite emissions (Fung et al. 1991). We include emissions from geological macroseeps (Kvenvolden and Rogers 2005; Etiope 2015). For *a priori* anthropogenic emissions we use the EDGAR v4.32 global emission inventory for 2012 (Janssens-Maenhout et al. 2019) that includes various sources related to human activities (e.g., oil and gas industry, coal mining, livestock, and waste).

We use monthly 3-D fields of OH, consistent with observed values for the lifetime of methyl chloroform, from the GEOS-Chem full chemistry simulation (Mao et al. 2013; Turner et al. 2015) to describe the main oxidation sink of methane. Using pre-computed fields of OH greatly simplifies our calculations. We examine the sensitivity of our results to different OH distributions, as described below. Additionally, in the next section, we describe a joint methane-OH inversion experiment from

which we also report results. We also include the net microbial consumption of methane in soil (Fung et al. 1991) and reaction with chlorine atoms (Thanwerdas et al. 2019).

To explore the sensitivity of our methane emission estimates for 2020 due to inferred reductions in OH due to large-scale industrial shutdown due to Covid-19 (Cooper et al. 2022) we also report *a posteriori* methane emission estimates that assume two different OH distributions, guided by observed changes in combustion and in tropospheric ozone. These sensitivity tests should not be considered as rigorous as our joint methane-OH inversion, described below, they represent a useful sanity check for our understanding.

First, we scale down our baseline monthly 3-D OH fields by 5% where combustion emissions of CO_2 (Oda and Maksyutov 2021) were larger than the mean emissions over Africa, resulting in reductions mainly between 15ºN and 65ºN. Our choice of 5% represents a reduction based on a recent study (Laughner et al. 2021). A recent study that accounted for reductions in nitrogen oxide emissions estimated a global OH reduction of ~4% due to Covid-19 lockdowns in 2020 (Miyazaki et al. 2021), which showed strong spatial and temporal variations, with localized reductions peaking at 20-30%. In the absence of direct measurements of OH and without considering co-reductions in non-methane hydrocarbons, these (and similar) results have large uncertainties.

Second, we assume a temporal-spatial distribution to describe the OH reduction in 2020, following a recent study on tropospheric ozone changes in 2020 and 2021 (Ziemke at al., 2022). First, we divide the world into regions: northern hemisphere (20°N-90°N) and the rest of the world. We assume the reduction in OH in the northern hemisphere starts from the boreal Spring of 2020 and peaks during the summer with a magnitude of 9% (blue line, Figure A1), higher than the ozone reduction found by Ziemke et al. (2022). For latitudes south of 20°N the time evolution of the reduction in ozone is less clear (Ziemke et al., 2022). We assume for simplicity that the OH reduction at these latitudes (red line, Figure A1) has a smaller peak value (-2.3%) and with a time lag of one month compared to the northern hemisphere region.

2.4 Ensemble Kalman filter inverse method

We use an ensemble Kalman Filter (EnKF) framework to estimate simultaneously CO_2 and methane fluxes from satellite measurements of the atmospheric CO_2 and methane (Feng, Palmer, Zhu, et al. 2022). Our state vector includes monthly scaling factors for 487 regional pulse-like basis functions (Figure A2) that describe CO_2 and methane fluxes, including 476 land regions and 11 oceanic regions. We define these land sub-regions by dividing the 11 TransCom–3 land regions into 42 nearly equal sub-regions, with the exception for temperate Eurasia that has been divided into 56 sub-regions due to its large landmass. We use the 11 oceanic regions defined by the TransCom–3 experiment. We use a 4-month moving lag window to reduce the computational costs for projecting the flux perturbation ensemble into observation space long after (>4 months) their emissions, beyond which time it is difficult to distinguish between the emitted signal from variations in the ambient background

atmosphere (Fraser et al. 2014a; Feng et al. 2017). Our *a priori* fluxes are described above. For simplicity we assume a fixed uncertainty of 40% for coefficients corresponding to the *a priori* CO_2 fluxes over each sub-region, and a larger uncertainty (60%) for the corresponding methane emissions. We also assume that *a priori* errors for the same gas are correlated with a spatial correlation length of 300 km and with a temporal correlation of one month.

As a sensitivity test, we also report methane fluxes inferred using the same EnKF approach but using the proxy GOSAT XCH_4 data and *in situ* methane data. These GOSAT XCH_4 retrievals are calculated from the XCH_4:XCO_2 ratio by applying an ensemble mean of model XCO_2, and then bias-corrected according to comparison with TCCON XCH_4 retrievals (R. J. Parker et al. 2020).

Currently there is no direct observation of the global distribution of atmospheric OH. Indirect constraints on atmospheric OH from the changing lifetimes of trace gases such as CO and methane are insufficient to determine 3-D distributions of OH. Here, we extend the inversion state vector to infer simultaneously methane emissions (as described above) and six OH scaling factors for *a priori* monthly 3-D OH fields from the atmospheric methane observations (section 2). These scaling factors correspond to six latitude bands: 75°S—50°S, 50°S—25°S, 25°S—0°, 0°—25°N, 25°N—50°N, 50°N—75°N. We do not consider scaling polar OH values. This calculation complements the OH sensitivity experiments described in the previous section. The Jacobian matrix, which describes the sensitivity of model methane concentrations to regional OH fields, is calculated with GEOS-Chem forced by *a priori* methane fluxes from the control run (Table 1) but with the OH climatology reduced by 5% for each of the six regions. To reduce the computational cost of this calculation, we use the same four-month lag window for the OH scaling factor estimates as for the methane emission estimates. So that each monthly OH scaling factor will be constrained only by observations in the subsequent four months, but its impact will remain for the entire experimental period. We used the OH climatology as our *a priori* and assume a uniform 3% uncertainty for each of the six regions so that the 2-sigma range covers possible OH changes that span ±6%. We use such a simple linearization scheme to adjust surface methane emissions and the monthly tropospheric OH by optimally fitting model calculations to atmospheric methane observations. We conduct the joint inversion for 2018 to 2021, including the six monthly OH scaling factors and methane emissions, and use the same atmospheric methane data used by the control calculation.

2.5 Correlative data

To help interpret the changes in methane emission estimates we use additional datasets that are relevant to microbial or pyrogenic production of methane. We use monthly surface temperature fields at a spatial resolution of 2°x2.5° from the Modern-Era Retrospective Analysis for Research and Applications, version 2 (MERRA2) developed by the Global Modeling and Assimilation Office, NASA Goddard Space Flight Center (Bosilovich *et al.*, 2015). Precipitation data are taken from the NOAA CMAP (CPC Merged Analysis of Precipitation) long-term global rainfall dataset (Xie and Arkin 1997) that provides near-global monthly coverage at a spatial resolution of 2.5° × 2.5°, from 1979 to near-present. In addition, we use monthly total

water storage (liquid water equivalent depth, LWE) on a 1° × 1° global grid from the NASA/DLR Gravity Recovery and Climate Experiment Follow-on (GRACE-FO) (Landerer et al. 2020). Finally, we explore monthly biomass burning emissions from the Global Fire Emissions Database (GFED v4) (van der Werf et al. 2017).

3 Results

Table 1 summarizes our global emission estimates inferred from GOSAT for 2020 and 2021; and for 2019, which we use as our baseline year throughout this study (Figure A3). The largest change in our global *a posteriori* emissions, corresponding to the OH climatology, occurs during 2019—2020 (27.0 Tg) from 583.7 to 610.7 Tg/yr. Our *a posteriori* emission estimates for 2019 and 2020 are within 2% of values reported by an independent study (Qu et al. 2022), consistent with our reported uncertainties. These elevated emissions are sustained, but not further increased, during 2021 (604.5 Tg/yr).

The 27.0 Tg emission increase in 2020 and the lack of further emissions growth in 2021 may appear inconsistent with the NOAA global annual mean growth rates of 15.19±0.41 ppb 18.12±0.47 ppb in 2020 and 2021, respectively (Table 1). Based on these reported atmospheric growth rates, and after considering the effects of methane sinks, we find that a one-box model calculation predicts an increase in emissions of 12.6 Tg between 2019 and 2020 and a further 15.1 Tg increase in 2021 (see Appendix B). These calculations use annual mean values that effectively represent the emissions increase between the middle of each successive year rather than the beginning and end. After considering the increases in monthly mean NOAA data, we find that the simple box model predicts a similar increase in emissions between December 2019 (583.7 Tg/yr) and December 2020 (610.1 Tg /yr) of 26.4 Tg /yr , with emissions thereafter stabilizing, with mean emissions of 610.1 Tg/yr in 2021. The resulting *a posteriori* model atmospheric methane concentrations agree well with the assimilated *in situ* data, as expected, but also reproduce the spatial and temporal variations of methane reported by the independent TCCON measurement network. As such, we conclude that the global mean emission results inferred from GOSAT are consistent with those inferred from NOAA surface data over multi-year periods, assuming a fixed methane atmospheric lifetime.

Figure 1b shows the broad geographical breakdown for our reported global changes in methane emissions. Relative to 2019, we find widespread increased emissions during 2020 except for China and India. Relative to baseline values in 2019 we see the largest annual increases in methane emissions during 2020 over Eastern Africa (14±3 Tg), tropical South America (5±3 Tg), tropical Asia (3±3 Tg), and temperate Eurasia (3±3 Tg), and the largest reductions over China (-6±3 Tg) and India (-2±3 Tg). We find comparable emission changes in 2021, relative to 2019, except for tropical and temperate South America where emissions increased by 9±4 Tg and 4±3 Tg, respectively, and for temperate North America where emissions increased by 5±2 Tg. Our results are broadly consistent with a recent study that showed that methane emissions inferred from TROPOMI were significantly higher in the first half of 2020 than during 2019 (McNorton et al. 2022). This study focused mainly on major countries, while we find the largest changes are over tropical latitudes where emissions in the second half of 2020 make significant contributions (Figure A4).

Figure 2 shows the distribution of methane emissions from 2020 and 2021 and the relative changes from our 2019 baseline year (Figure A3a). During 2020, there are significant decreases (20-30%) over the manufacturing regions such as eastern China, India, central America, and eastern Europe. There are also significant increases across Eastern Africa (30-40%), eastern North America (30%), and maritime Southeast Asia (30%). During 2021, we see similar changes in emissions, but they are typically exaggerated. There is more of a pronounced increase over Eastern Africa (>50%), southern Brazil (50%), and eastern North America (up to 40%), and large decreases over eastern China (-50%) and western Russia (-50%). During 2021 there is also a large decrease over equatorial West Africa and eastern Europe (Figure 1b). There are substantial seasonal changes in methane emissions (Figure A4) that are broadly consistent with seasonal changes in temperature and rainfall (not shown). Using methane columns determined by the proxy data, assuming model values for CO_2 (R. J. Parker et al. 2020), we find results for 2020 and 2021 that are generally within ten percent of the values we report using the proxy data directly (Figure A5 and Figure A6).

Figure 3 shows different annual surface temperature warming patterns in 2020 and 2021. During 2020 the high northern latitudes are dominated by summer warming over Siberia (2-3 K on an annual scale) that has been linked to greenhouse gas emissions (Ciavarella et al. 2021) and surface temperatures over Alaska were 2-3 K cooler than baseline values in 2019, where there were comparatively small changes in groundwater (< 5 cm). North America, western Europe and Scandinavia also experienced anomalously warm annual mean temperatures (typically within ±2 K of 2019 values). There were smaller changes in temperatures at low latitudes (typically ±1 K of 2019 values), but larger increases in groundwater (±10-20 cm) associated with higher changes in rainfall (Figure A7), particularly over Eastern Africa and eastern Brazil. During 2021, high northern latitudes were cooler than 2019 (<2-3 K) except for the contiguous US and Canada (higher than 2019 values by 2-3 K). Midlatitudes and low latitudes generally did not experience the warm temperatures of 2020. Elevated groundwater was sustained in 2021 over East and Southern Africa, eastern tropical South America (principally Brazil but stretching up to Venezuela), central America, India, maritime Southeast Asia, and north and southeast Australia. Groundwater decreased over the contiguous US, part of tropical South America and parts of Eurasia. We find generally stronger annual and seasonal relationships between methane emission anomalies and hydrological anomalies (rainfall and groundwater) for 2020 and 2021 (Figure 3) than for temperature anomalies. Particularly, we find statistically significant large-scale positive correlations (typically 0.6-0.9; $p<0.001$) for all seasons between methane and groundwater anomalies over Eastern Africa, tropical South America, and tropical Asia (Figure 4), but no significant correlation between methane and surface temperature anomalies (not shown). This is consistent with recent studies that have highlighted an increasing role for microbial sources in the tropical methane budget (Lunt et al. 2019; Feng, Palmer, Zhu, et al. 2022; Wilson et al. 2020). Over North America, we find a significant negative correlation (from -0.3 to -0.6; $p<0.001$) with rainfall during MAM and JJA and a significant positive correlation with temperature during JJA (0.4; $p < 0.001$), which we do not currently understand. Fire emissions did not increase

much where we report the largest increases in methane emissions in 2020 or 2021, except over central Canadian provinces. (Figure A7).

By including OH scaling factors into our state vector, we infer simultaneously OH distributions and methane emissions (section 2.4). Table 1 reports the resulting annual changes in tropospheric OH. The annual mean *a posteriori* OH changes relative to climatological *a priori* values are 0.91±1.7%, -0.52±1.7% and 0.62±1.7% for 2019, 2020, and 2021, respectively (Table 1). These values correspond to *a posteriori* OH reductions of 1.43% and 0.29% in 2020 and 2021 relative to the 2019 baseline year (Figure A3b). Table 1 shows that these reductions in OH correspond to smaller *a posteriori* methane emissions needed to fit the observations, as expected. For 2019 we estimate a 0.3% higher value for the *a posteriori* methane emission compared the OH climatology inversion. In 2020, we require an emission increase of 17.9 Tg relative to 2019, an approximate drop of a third in the emission growth needed to reconcile atmospheric observations relative to the OH climatology inversion (Table 1). However, in 2021 we require only a small emission increase of 0.5 Tg (8%) from 2020 due to a concomitant increase in OH compared to a decrease of 6.2 Tg in 2021 for the inversion using OH climatology (Table 1).

Figure 5 shows that annual *a posteriori* error correlations between the six OH scaling factors and the regional methane emission estimates are only weakly correlated (ranging ±0.1, and typically less than ±0.05), suggesting that the GOSAT methane data support the estimation of OH scaling factors on our large geographical scales. Our joint methane-OH inversion results for 2020 are consistent with our simpler OH perturbation studies, described in section 2.3, that are reported in Table 2. For these sensitivity experiments, we find that we need reduced increases in methane emissions in 2020, ranging between -22.6% and -27.4%. They provide confidence in our *a posteriori* emission estimates and in our statement that most of the atmospheric methane growth in 2020 was due to an increase in emissions, with the OH reduction associated with the Covid-19 lockdowns representing approximately 30% of the global atmospheric methane growth.

Figure 1c and Figure 6 show the geographical distribution of methane emissions for 2020 and 2021 corresponding to the joint methane-OH inversion and how they differ from *a posteriori* methane emissions inferred from OH fixed climatology. Figure 7 shows the corresponding *a posteriori* methane loss due to OH oxidation from the joint methane-OH inversion relative to the baseline inversion that uses OH climatology. Strictly speaking, we cannot easily compare results from the two inversions because the differences are relative to their own pre-2020 baselines (Figure A3). The 2019 baseline for the joint methane-OH inversion is lower over eastern China, eastern India, and some of boreal Eurasia, and higher over parts of tropical and temperate South America and maritime Southeast Asia (Figure A3). Differences between the inversions are typically much smaller than 10% of the fluxes. Nevertheless, our main conclusions remain robust for both inversions.

Eastern Africa remains the biggest contributor to atmospheric methane growth in 2020 and 2021 but with the estimated emission increase reduced by ~15%, as expected, given the decrease in OH (Figure 1c). A notable difference includes a large

drop in emissions over tropical South America in 2020 but this partially recovers in 2021 (Figure 1c). The difference between the two inversions for tropical South America in 2020 can be attributed to a decrease in the methane loss due to OH oxidation in the north of that region (Figure 7) but also the higher 2019 baseline for the joint methane-OH inversion (Figure A3b) that effectively reduces the emission increase needed to reconcile with observations (Figure 6). This argument is also relevant to smaller *a posteriori* methane emissions for the joint methane-OH inversion over Southeast Asia and Southeast Australia (Figures 1c, 6, A3). A lower 2019 baseline over China and India for the joint methane-OH inversion (Figure A3) results in small reductions in *a posteriori* methane emissions needed to reconcile with observations (Figures 1c, 6). A similar argument associated with a lower 2019 baseline value for the joint methane-OH inversion helps to explain the increase in *a posteriori* methane emissions over temperate North America and Europe in both years (Figures 1c, 6).

Our *a posteriori* emission estimates from our baseline inversion that uses climatological OH values and from joint methane-OH inversion are consistent with independent observations from the TCCON network (Figures C1 and C2). *A posteriori* methane emission estimates for the joint methane-OH inversion generally has slightly smaller differences at southern and northern midlatitude latitude sites (within 1 ppb) but does slightly worse (within 3 ppb) for the Bremen (Br), Karlsruhe (Ka), and Paris sites. Both inversions have comparable standard deviation about the mean differences that are typically within 10 ppb.

4 Concluding Remarks

We reported regional emission estimates of methane during 2020 and 2021, two years with record-breaking atmospheric growth rates, inferred from satellite observations of methane from the Japanese Greenhouse gases Observing SATellite. For our control inversion we used fixed climatological OH values. Substantial, widespread reductions in nitrogen oxides during 2020 associated with the shutdown of manufacturing and other industries will have perturbed atmospheric concentrations of the OH loss of methane. A reduction in OH could also help explain, in principle, the record-breaking atmospheric increase in methane. To address this point, we also report *a posteriori* zonal mean OH scaling factors that form part of a joint methane-OH inversion. Generally, we find our results from the joint-OH inversion are broadly consistent with our idealized sensitivity calculations that describe changes in OH informed by distributions in anthropogenic emission and the response of tropospheric ozone, resulting in a reduced emission growth of 17.9 Tg/yr in 2020 that represents 66% of our baseline inversion.

We find that emissions from Eastern Africa, tropical South America, and temperate North America play a significant role in determining the global atmospheric growth rate of methane in one or both years. The contribution from Eastern Africa dominates the global growth and is consistent with previous studies that have reported emissions from recent years (Feng, Palmer, Zhu, et al. 2022; Pandey et al. 2021; Lunt et al. 2021a; 2019), ranging from 13 to 14 Tg in 2020 and 2021, relative to the 2019 baseline year. The magnitude of this increase in regional emission is reduced by approximately ~15% due to a 4% reduction in OH, as expected. The influence of tropical South America and temperate North America is sensitive to the OH

distribution, particularly during 2020. The joint methane-OH inversion results in a substantial decrease in emissions over tropical South America but this largely recovers by 2021. We find that the joint-OH inversion leads to an increase in northern midlatitude methane emissions from temperate North America, temperate Eurasia, and Europe due to a 0.3% increase in OH. We also find that adjusting OH results in smaller emissions reductions from China in 2020 and 2021 and a smaller increase in emissions from Southeast Asia. We find statistically significant positive correlations between tropical methane emission and hydrological anomalies, consistent with recent studies that have highlighted a growing role for microbial sources over the tropics (Lunt et al. 2019; Feng, Palmer, Zhu, et al. 2022; Wilson et al. 2020).

Our results are broadly consistent with a recent study of the 2020 period (Qu et al. 2022), including the magnitude of change associated with a change in OH, albeit concluded using an independent method. Recent work that used *in situ* methane data reported a smaller increase in methane emissions during 2020 (Peng et al. 2022), consistent with poor data coverage over the tropics as we explain in Appendix B. Their estimate for the Covid-19-related OH reduction during 2020 (1.6%) is consistent with our estimate but because they used only surface data in their inversion, they underestimated the atmospheric methane growth from 2019 to 2020 (Table 1) and consequently overestimated the influence of reduced OH on the atmospheric growth rate of methane during 2020.

Our study highlights the tremendous value of using satellite observations to understand rapid changes in atmospheric methane. They provide crucial information not only to identify regional column hotspots associated with emissions but also provide correlative information to help attribute those hotspots to specific anthropogenic or natural emissions. Our study also illustrates the importance of simultaneously estimating methane emissions and changes in OH to improve quantitative knowledge of changes in methane emissions, which is necessary to attribute global atmospheric growth to individual source regions.

Data availability. The University of Leicester GOSAT Proxy v9.0 XCH_4 data are available from the Centre for Environmental Data Analysis data repository at https://doi.org/10.5285/18ef8247f52a4cb6a14013f8235cc1eb. Precipitation, temperature, and the GRACE datasets are available at http://grace.jpl.nasa.gov. The community-led GEOS-Chem model of atmospheric chemistry and model is maintained centrally by Harvard University (http://geos-chem.seas.harvard.edu), and is available on request. The ensemble Kalman filter code is publicly available as PyOSSE (https://www.nceo.ac.uk/data-tools/atmospheric-tools/). The TCCON data were obtained from the TCCON Data Archive hosted by CaltechDATA at https://tccondata.org. CH_4 GLOBALVIEWplus v5.0 ObsPack is available from https://search.datacite.org/works/10.25925/20221001, and CO_2 GLOBALVIEWplus v8.0 ObsPack is available from https://search.datacite.org/works/10.25925/20220808.

Author contributions. LF and PIP designed the research; LF and MFL prepared the calculations; RJP and HB provided the GOSAT data and expert advice on its usage; PIP wrote the paper, with comments from LF, RJP, MFL, and HB.

Competing interests. The contact author has declared that neither they nor their co-authors have any competing interests.

Acknowledgements: We thank the Japanese Aerospace Exploration Agency, National Institute for Environmental Studies, and the Ministry of Environment for the GOSAT data and their continued support as part of the Joint Research Agreements at the Universities of Edinburgh and Leicester. GOSAT retrievals were processed using the ALICE High-Performance Computing Facility at the University of Leicester. We thank all the scientists that submitted data to the CO_2 and methane Observation Package (ObsPack) data products, coordinated by NOAA ESRL, and making them freely available for carbon cycle research. We also thank the GEOS-Chem community, particularly the team at Harvard University who help maintain the GEOS-Chem model, and the NASA Global Modeling and Assimilation Office (GMAO) who provide the MERRA2 data product.

Financial support: L.F., P.I.P., R.J.P., and H.B. acknowledge support from the UK National Centre for Earth Observation funded by the National Environment Research Council (NE/R016518/1); R.J.P. also acknowledges funding from grant NE/N018079/1. We acknowledge funding from the Copernicus Climate Change Service (C3S2_312a_Lot2) related to generation of the GOSAT data.

References

Bloom, A A, K W Bowman, M Lee, A J Turner, R Schroeder, J R Worden, R Weidner, K C McDonald, and D J Jacob. 2017. "A Global Wetland Methane Emissions and Uncertainty Dataset for Atmospheric Chemical Transport Models (WetCHARTs Version 1.0)." *Geoscientific Model Development* 10 (6): 2141–56. https://doi.org/10.5194/gmd-10-2141-2017.

Bosilovich, M. G, S Akella, L Coy, R Cullather, C Draper, R Gelaro, R Kovach, et al. 2015. "MERRA-2: Initial Evaluation of the Climate."

Buschmann, M, C Petri, M Palm, T Warneke, and J Notholt. 2022. "TCCON Data from Ny-Ålesund, Svalbard (NO), Release GGG2020.R0." CaltechDATA. https://doi.org/10.14291/tccon.ggg2020.nyalesund01.R0.

Ciavarella, Andrew, Daniel Cotterill, Peter Stott, Sarah Kew, Sjoukje Philip, Geert Jan van Oldenborgh, Amalie Skålevåg, et al. 2021. "Prolonged Siberian Heat of 2020 Almost Impossible without Human Influence." *Climatic Change* 166 (1): 9.

Cooper, Matthew J., Randall V. Martin, Melanie S. Hammer, Pieternel F. Levelt, Pepijn Veefkind, Lok N. Lamsal, Nickolay A. Krotkov, Jeffrey R. Brook, and Chris A. McLinden. 2022. "Global Fine-Scale Changes in Ambient NO_2 during COVID-19 Lockdowns." *Nature* 601 (7893). https://doi.org/10.1038/s41586-021-04229-0.

Cox, Adam, Alcide Giorgio Di Sarra, Anna Karion, Arlyn Andrews, Aurelie Colomb, Bert Scheeren, Bill Paplawsky, et al. 2022. "Multi-Laboratory Compilation of Atmospheric Carbon Dioxide Data for the Year 2021;

Obspack_co2_1_NRT_v7.1_2022-03-04." NOAA Earth System Research Laboratory, Global Monitoring Laboratory. https://doi.org/10.25925/20220301.

Cox, Adam, Alcide Giorgio Di Sarra, Alex Vermeulen, Alistair Manning, Andreas Beyersdorf, Andreas Zahn, Andrew Manning, et al. 2021. "Multi-Laboratory Compilation of Atmospheric Carbon Dioxide Data for the Period 1957-2020; Obspack_co2_1_GLOBALVIEWplus_v7.0_2021-08-18." NOAA Global Monitoring Laboratory. https://doi.org/10.25925/20210801.

———. 2022. "Multi-Laboratory Compilation of Atmospheric Carbon Dioxide Data for the Period 1957-2021; Obspack_co2_1_GLOBALVIEWplus_v8.0_2022-08-27." NOAA Global Monitoring Laboratory. https://doi.org/10.25925/20220808.

Etiope, E. 2015. *Natural Gas Seepage: The Earth's Hydrocarbon Degassing*. Springer.

Feng, L., Paul I Palmer, Hartmut Bösch, Robert J Parker, Alex J Webb, Caio S C Correia, Nicholas M Deutscher, et al. 2017. "Consistent Regional Fluxes of CH_4 and CO_2 Inferred from GOSAT Proxy XCH_4: XCO_2 Retrievals, 2010--2014." *Atmos. Chem. Phys* 17: 4781–97.

Feng, L., Paul I Palmer, Sihong Zhu, Robert J Parker, and Yi Liu. 2022. "Tropical Methane Emissions Explain Large Fraction of Recent Changes in Global Atmospheric Methane Growth Rate." *Nature Communications* 13 (1): 1378. https://doi.org/10.1038/s41467-022-28989-z.

Feng, L, P I Palmer, R J Parker, M F Lunt, and H Boesch. 2022. "Methane Emissions Responsible for Record-Breaking Atmospheric Methane Growth Rates in 2020 and 2021." *Atmos. Chem. Phys. Discuss.* 2022 (June): 1–23. https://doi.org/10.5194/acp-2022-425.

Fraser, A., P. I. Palmer, L. Feng, H. Bösch, R. Parker, E. J. Dlugokencky, P. B. Krummel, and R. L. Langenfelds. 2014a. "Estimating Regional Fluxes of CO_2 and CH_4 Using Space-Borne Observations of XCH_4: XCO_2." *Atmospheric Chemistry and Physics* 14 (23). https://doi.org/10.5194/acp-14-12883-2014.

Fraser, A, P I Palmer, L Feng, H Bösch, R Parker, E J Dlugokencky, P B Krummel, and R L Langenfelds. 2014b. "Estimating Regional Fluxes of CO_2 and CH_4 Using Space-Borne Observations of XCH_4: XCO_2." *Atmospheric Chemistry and Physics* 14 (23): 12883–95. https://doi.org/10.5194/acp-14-12883-2014[FL1].

Fung, I, J John, J Lerner, E Matthews, M Prather, L P Steele, and P J Fraser. 1991. "Three-Dimensional Model Synthesis of the Global Methane Cycle." *Journal of Geophysical Research: Atmospheres* 96 (D7): 13033–65. https://doi.org/https://doi.org/10.1029/91JD01247.

García, O E, M Schneider, B Herkommer, J Gross, F Hase, T Blumenstock, and E Sepúlveda. 2022. "TCCON Data from Izana (ES), Release GGG2020.R1." CaltechDATA. https://doi.org/10.14291/tccon.ggg2020.izana01.R1.

Gurney, Kevin Robert, Rachel M Law, A Scott Denning, Peter J Rayner, Bernard C Pak, David Baker, Philippe Bousquet, et al. 2004. "Transcom 3 Inversion Intercomparison: Model Mean Results for the Estimation of Seasonal Carbon Sources and Sinks." *Global Biogeochemical Cycles* 18 (1).

Hase, F, B Herkommer, J Groß, T Blumenstock, M.ä. Kiel, and S Dohe. 2022. "TCCON Data from Karlsruhe (DE), Release

GGG2020.R0." CaltechDATA. https://doi.org/10.14291/tccon.ggg2020.karlsruhe01.R0.

Janssens-Maenhout, G, M Crippa, D Guizzardi, M Muntean, E Schaaf, F Dentener, P Bergamaschi, et al. 2019. "EDGAR v4.3.2 Global Atlas of the Three Major Greenhouse Gas Emissions for the Period 1970--2012." *Earth System Science Data* 11 (3): 959–1002. https://doi.org/10.5194/essd-11-959-2019.

Kivi, R, P Heikkinen, and E Kyrö. 2022. "TCCON Data from Sodankylä (FI), Release GGG2020.R0." CaltechDATA. https://doi.org/10.14291/tccon.ggg2020.sodankyla01.R0.

Kvenvolden, K A, and B W Rogers. 2005. "Gaia's Breath's Global Methane Exhalations." *Marine and Petroleum Geology* 22 (4): 579–90. https://doi.org/https://doi.org/10.1016/j.marpetgeo.2004.08.004.

Landerer, Felix W, Frank M Flechtner, Himanshu Save, Frank H Webb, Tamara Bandikova, William I Bertiger, Srinivas V Bettadpur, et al. 2020. "Extending the Global Mass Change Data Record: {GRACE} Follow-On Instrument and Science Data Performance." *Geophysical Research Letters* 47 (12). https://doi.org/10.1029/2020gl088306.

Laughner, Joshua L., Jessica L. Neu, David Schimel, Paul O. Wennberg, Kelley Barsanti, Kevin W. Bowman, Abhishek Chatterjee, et al. 2021. "Societal Shifts Due to COVID-19 Reveal Large-Scale Complexities and Feedbacks between Atmospheric Chemistry and Climate Change." *Proceedings of the National Academy of Sciences of the United States of America* 118 (46). https://doi.org/10.1073/pnas.2109481118.

Liu, Cheng, Wei Wang, Youwen Sun, and Changgong Shan. 2022. "TCCON Data from Hefei (PRC), Release GGG2020.R0." CaltechDATA. https://doi.org/10.14291/tccon.ggg2020.hefei01.R0.

Lunt, M. F., P I Palmer, L Feng, C M Taylor, H Boesch, and R J Parker. 2019. "An Increase in Methane Emissions from Tropical Africa between 2010 and 2016 Inferred from Satellite Data." *Atmos. Chem. Phys.* 19 (23): 14721–40. https://doi.org/10.5194/acp-19-14721-2019.

Lunt, M F, P I Palmer, A Lorente, T Borsdorff, J Landgraf, R J Parker, and H Boesch. 2021. "Rain-Fed Pulses of Methane from East Africa during 2018-2019 Contributed to Atmospheric Growth Rate." *Environmental Research Letters* 16 (2): 24021. https://doi.org/10.1088/1748-9326/abd8fa.

Mao, Jingqiu, Fabien Paulot, Daniel J Jacob, Ronald C Cohen, John D Crounse, Paul O Wennberg, Christoph A Keller, Rynda C Hudman, Michael P Barkley, and Larry W Horowitz. 2013. "Ozone and Organic Nitrates over the Eastern United States: Sensitivity to Isoprene Chemistry." *Journal of Geophysical Research: Atmospheres* 118 (19): 11,211-256,268. https://doi.org/https://doi.org/10.1002/jgrd.50817.

Mazière, M De, M K Sha, F Desmet, C Hermans, F Scolas, N Kumps, M Zhou, J.-M. Metzger, V Duflot, and J.-P. Cammas. 2022. "TCCON Data from Réunion Island (RE), Release GGG2020.R0." CaltechDATA. https://doi.org/10.14291/tccon.ggg2020.reunion01.R0.

McNorton, J, N Bousserez, A Agustí-Panareda, G Balsamo, L Cantarello, R Engelen, V Huijnen, et al. 2022. "Quantification of Methane Emissions from Hotspots and during COVID-19 Using a Global Atmospheric Inversion." *Atmos. Chem. Phys.* 22 (9): 5961–81. https://doi.org/10.5194/acp-22-5961-2022.

Miyazaki, Kazuyuki, Kevin Bowman, Takashi Sekiya, Masayuki Takigawa, Jessica L. Neu, Kengo Sudo, Greg Osterman, and

Henk Eskes. 2021. “Global Tropospheric Ozone Responses to Reduced NOx Emissions Linked to the COVID-19 Worldwide Lockdowns.” *Science Advances* 7 (24). https://doi.org/10.1126/sciadv.abf7460.

Morino, I., Voltaire A Velazco, Akihiro Hori, Osamu Uchino, and David W T Griffith. 2022. “TCCON Data from Burgos, Ilocos Norte (PH), Release GGG2020.R0.” CaltechDATA. https://doi.org/10.14291/tccon.ggg2020.burgos01.R0.

Morino, I, H Ohyama, A Hori, and H Ikegami. 2022a. “TCCON Data from Rikubetsu (JP), Release GGG2020.R0.” CaltechDATA. https://doi.org/10.14291/tccon.ggg2020.rikubetsu01.R0.

———. 2022b. “TCCON Data from Tsukuba (JP), 125HR, Release GGG2020.R0.” CaltechDATA. https://doi.org/10.14291/tccon.ggg2020.tsukuba02.R0.

Notholt, J, C Petri, T Warneke, and M Buschmann. 2022. “TCCON Data from Bremen (DE), Release GGG2020.R0.” CaltechDATA. https://doi.org/10.14291/tccon.ggg2020.bremen01.R0.

Oda, T, and S Maksyutov. 2021. “ODIAC Fossil Fuel CO_2 Emissions Dataset (Version Name: ODIAC2020b).” Center for Global Environmental Research, National Institute for Environmental Studies. https://doi.org/10.17595/20170411.001.

Palmer, P I, L Feng, M F Lunt, R J Parker, H Bösch, X Lan, L Alba, and B Tobiaa. 2021. “The Added Value of Satellite Observations of Methane for Understanding the Contemporary Methane Budget.” *Phil. Trans. R. Soc. A.* 379 (20210106). https://doi.org/http://doi.org/10.1098/rsta.2021.0106.

Pandey, Sudhanshu, Sander Houweling, Maarten Krol, Ilse Aben, Guillaume Monteil, Narcisa Nechita-Banda, Edward J Dlugokencky, et al. 2017. “Enhanced Methane Emissions from Tropical Wetlands during the 2011 La Niña.” *Scientific Reports* 7 (1). https://doi.org/10.1038/srep45759.

Pandey, Sudhanshu, Sander Houweling, Alba Lorente, Tobias Borsdorff, Maria Tsivlidou, A. Anthony Bloom, Benjamin Poulter, Zhen Zhang, and Ilse Aben. 2021. “Using Satellite Data to Identify the Methane Emission Controls of South Sudan’s Wetlands.” *Biogeosciences*. https://doi.org/10.5194/bg-18-557-2021.

Parker, R., and Hartmut Boesch. 2020. “University of Leicester GOSAT Proxy XCH4 v9.0.” Centre for Environmental Data Analysis.

Parker, R J, Alex Webb, Hartmut Boesch, Peter Somkuti, Rocio Barrio Guillo, Antonio Di Noia, Nikoleta Kalaitzi, et al. 2020. “A Decade of GOSAT Proxy Satellite CH_4 Observations.” *Earth System Science Data* 12 (4). https://doi.org/10.5194/essd-12-3383-2020.

Peng, Shushi, Xin Lin, Rona L Thompson, Yi Xi, Gang Liu, Didier Hauglustaine, Xin Lan, et al. 2022. “Wetland Emission and Atmospheric Sink Changes Explain Methane Growth in 2020.” *Nature* 612 (7940): 477–82. https://doi.org/10.1038/s41586-022-05447-w.

Petri, Christof, Mihalis Vrekoussis, Constantina Rousogenous, Thorsten Warneke, Jean Sciare, and Justus Notholt. 2022. “TCCON Data from Nicosia (CY), Release GGG2020.R0.” CaltechDATA. https://doi.org/10.14291/tccon.ggg2020.nicosia01.R0.

Pollard, David Frank, John Robinson, and Hisako Shiona. 2022. “TCCON Data from Lauder (NZ), Release GGG2020.R0.” CaltechDATA. https://doi.org/10.14291/tccon.ggg2020.lauder03.R0.

Qu, Zhen, Daniel J Jacob, Yuzhong Zhang, Lu Shen, Daniel J Varon, Xiao Lu, Tia Scarpelli, Anthony Bloom, John Worden, and Robert J Parker. 2022. "Attribution of the 2020 Surge in Atmospheric Methane by Inverse Analysis of GOSAT Observations." *Environmental Research Letters* 17 (9): 094003. https://doi.org/10.1088/1748-9326/ac8754.

Randerson, James T., Matthew V. Thompson, Carolyn M. Malmstrom, Christopher B. Field, and Inez Y. Fung. 1996. "Substrate Limitations for Heterotrophs: Implications for Models That Estimate the Seasonal Cycle of Atmospheric CO2." *Global Biogeochemical Cycles* 10 (4). https://doi.org/10.1029/96GB01981.

Rigby, M, R G Prinn, P J Fraser, P G Simmonds, R L Langenfelds, J Huang, D M Cunnold, et al. 2008. "Renewed Growth of Atmospheric Methane." *Geophysical Research Letters* 35 (22). https://doi.org/https://doi.org/10.1029/2008GL036037.

Sarra, Alcide Giorgio Di, Ankur Desai, Anna Karion, Arlyn Andrews, Aurelie Colomb, Bert Scheeren, Brian Viner, et al. 2022. "Multi-Laboratory Compilation of Atmospheric Methane Data for the Year 2021; Obspack_ch4_1_NRT_v4.0_2022-03-03." NOAA Earth System Research Laboratory, Global Monitoring Laboratory. https://doi.org/10.25925/20211101.

Sarra, Alcide Giorgio Di, Andreas Zahn, Andrew Watson, Ankur Desai, Anna Karion, Arlyn Andrews, Aurelie Colomb, et al. 2021. "Multi-Laboratory Compilation of Atmospheric Methane Data for the Period 1983-2020; Obspack_ch4_1_GLOBALVIEWplus_v4.0_2021-10-14." NOAA Global Monitoring Laboratory. https://doi.org/10.25925/20211001.

Shiomi, K, S Kawakami, H Ohyama, K Arai, H Okumura, H Ikegami, and M Usami. 2022. "TCCON Data from Saga (JP), Release GGG2020.R0." CaltechDATA. https://doi.org/10.14291/tccon.ggg2020.saga01.R0.

Takahashi, Taro, Stewart C Sutherland, Rik Wanninkhof, Colm Sweeney, Richard A Feely, David W Chipman, Burke Hales, et al. 2009. "Climatological Mean and Decadal Change in Surface Ocean PCO2, and Net Sea-Air CO_2 Flux over the Global Oceans." *Deep Sea Research Part II: Topical Studies in Oceanography* 56 (8): 554–77. https://doi.org/https://doi.org/10.1016/j.dsr2.2008.12.009.

Té, Y, P Jeseck, and C Janssen. 2022. "TCCON Data from Paris (FR), Release GGG2020.R0." CaltechDATA. https://doi.org/10.14291/tccon.ggg2020.paris01.R0.

Thanwerdas, J, M Saunois, A Berchet, I Pison, D Hauglustaine, M Ramonet, C Crevoisier, B Baier, C Sweeney, and P Bousquet. 2019. "Impact of Atomic Chlorine on the Modelling of Total Methane and Its ^{13}C:^{12}C Isotopic Ratio at Global Scale." *Atmospheric Chemistry and Physics Discussions* 2019: 1–28. https://doi.org/10.5194/acp-2019-925.

Turner, A J, D J Jacob, K J Wecht, J D Maasakkers, E Lundgren, A E Andrews, S C Biraud, et al. 2015. "Estimating Global and North American Methane Emissions with High Spatial Resolution Using GOSAT Satellite Data." *Atmospheric Chemistry and Physics* 15 (12): 7049–69. https://doi.org/10.5194/acp-15-7049-2015.

Warneke, T, C Petri, J Notholt, and M Buschmann. 2022. "TCCON Data from Orléans (FR), Release GGG2020.R0." CaltechDATA. https://doi.org/10.14291/tccon.ggg2020.orleans01.R0.

Wennberg, P O, C M Roehl, D Wunch, J.-F. Blavier, G C Toon, N T Allen, R Treffers, and J Laughner. 2022. "TCCON Data from Caltech (US), Release GGG2020.R0." CaltechDATA. https://doi.org/10.14291/tccon.ggg2020.pasadena01.R0.

Wennberg, P O, C M Roehl, D Wunch, G C Toon, J.-F. Blavier, R Washenfelder, G Keppel-Aleks, and N T Allen. 2022. "TCCON Data from Park Falls (US), Release GGG2020.R0." CaltechDATA. https://doi.org/10.14291/tccon.ggg2020.parkfalls01.R0.

Wennberg, P O, D Wunch, C M Roehl, J.-F. Blavier, G C Toon, and N T Allen. 2022. "TCCON Data from Lamont (US), Release GGG2020.R0." CaltechDATA. https://doi.org/10.14291/tccon.ggg2020.lamont01.R0.

Werf, G R van der, J T Randerson, L Giglio, T T van Leeuwen, Y Chen, B M Rogers, M Mu, et al. 2017. "Global Fire Emissions Estimates during 1997--2016." *Earth System Science Data* 9 (2): 697–720. https://doi.org/10.5194/essd-9-697-2017.

Wilson, C, M P Chipperfield, M Gloor, R J Parker, H Boesch, J McNorton, L V Gatti, J B Miller, L S Basso, and S A Monks. 2020. "Large and Increasing Methane Emissions from Eastern Amazonia Derived from Satellite Data, 2010--2018." *Atmospheric Chemistry and Physics Discussions* 2020: 1–38. https://doi.org/10.5194/acp-2020-1136.

Wunch, D, J Mendonca, O Colebatch, N T Allen, J.-F. Blavier, K Kunz, S Roche, et al. 2022. "TCCON Data from East Trout Lake, SK (CA), Release GGG2020.R0." CaltechDATA. https://doi.org/10.14291/tccon.ggg2020.easttroutlake01.R0.

Xie, P, and P A Arkin. 1997. "'Global Precipitation: A 17-Year Monthly Analysis Based on Gauge Observations, Satellite Estimates, and Numerical Model Outputs.'" *Bulletin of the American Meteorological Society* 78 (11): 2539–58. https://doi.org/10.1175/1520-0477(1997)078<2539:GPAYMA>2.0.CO;2.

Zhou, Minqiang, Pucai Wang, Nicolas Kumps, Christian Hermans, and Weidong Nan. 2022. "TCCON Data from Xianghe, China, Release GGG2020.R0." CaltechDATA. https://doi.org/10.14291/tccon.ggg2020.xianghe01.R0.

Ziemke, Jerry R, Natalya A Kramarova, Stacey M Frith, Liang-Kang Huang, David P Haffner, Krzysztof Wargan, Lok N Lamsal, Gordon J Labow, Richard D McPeters, and Pawan K Bhartia. 2022. "NASA Satellite Measurements Show Global-Scale Reductions in Free Tropospheric Ozone in 2020 and Again in 2021 During COVID-19." *Geophysical Research Letters* 49 (15): e2022GL098712. https://doi.org/https://doi.org/10.1029/2022GL098712.

Figures

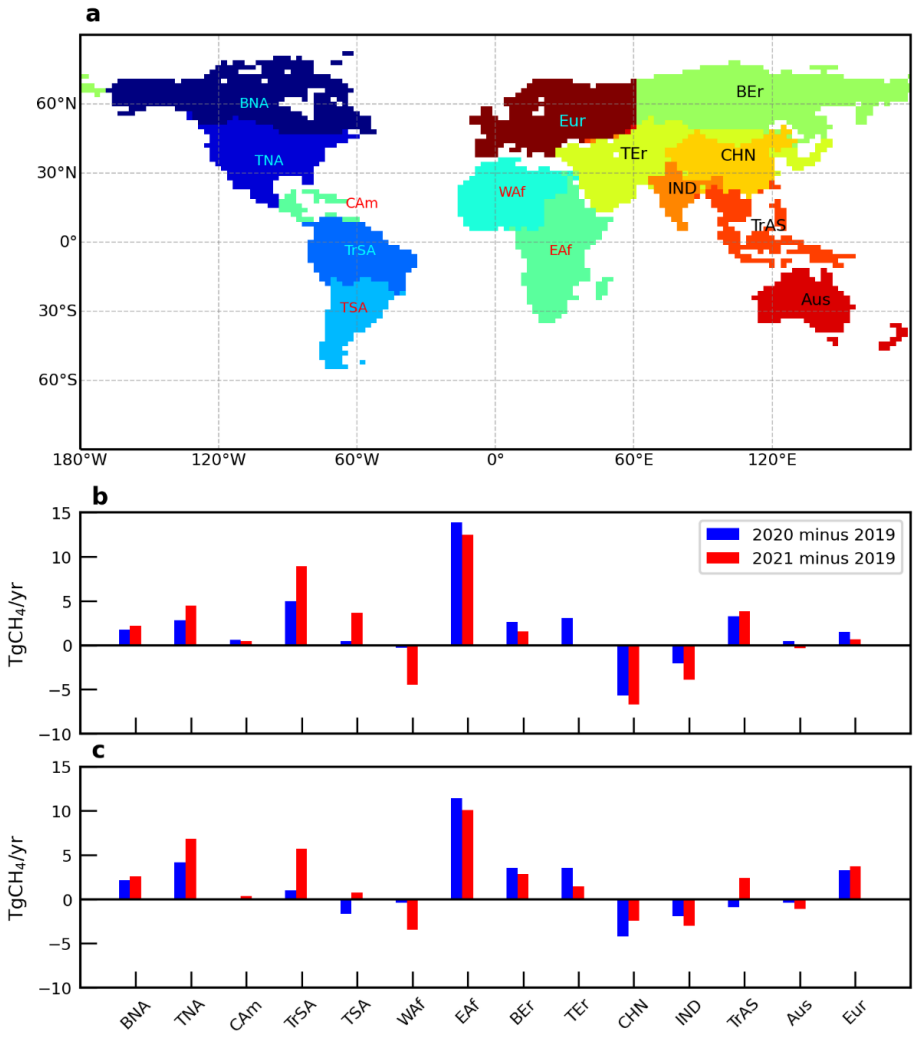

Figure 1 Large-scale geographical regions a) for which we report methane changes ($TgCH_4/yr$) in 2020 and 2021 b) differences between *a posteriori* emissions from 2020 and 2021 relative to inversion-specific baselines for 2019. Geographical regions, informed by TransCom-3 experiments (Gurney et al. 2004), include boreal North America (BNA), temperate North America (TNA), central America (Cam), tropical South America (TrSA), temperature South America (TSA), Europe (Eur), western Africa (WAf), eastern Africa (EAf), boreal Eurasia (BEr), temperate Eurasia (TEr), India (IND), China (CHN), tropical Asia (TrAs), and Australia (Aus). Panel c) is the same as b) but for *a posteriori* methane emission from the joint methane-OH inversion.

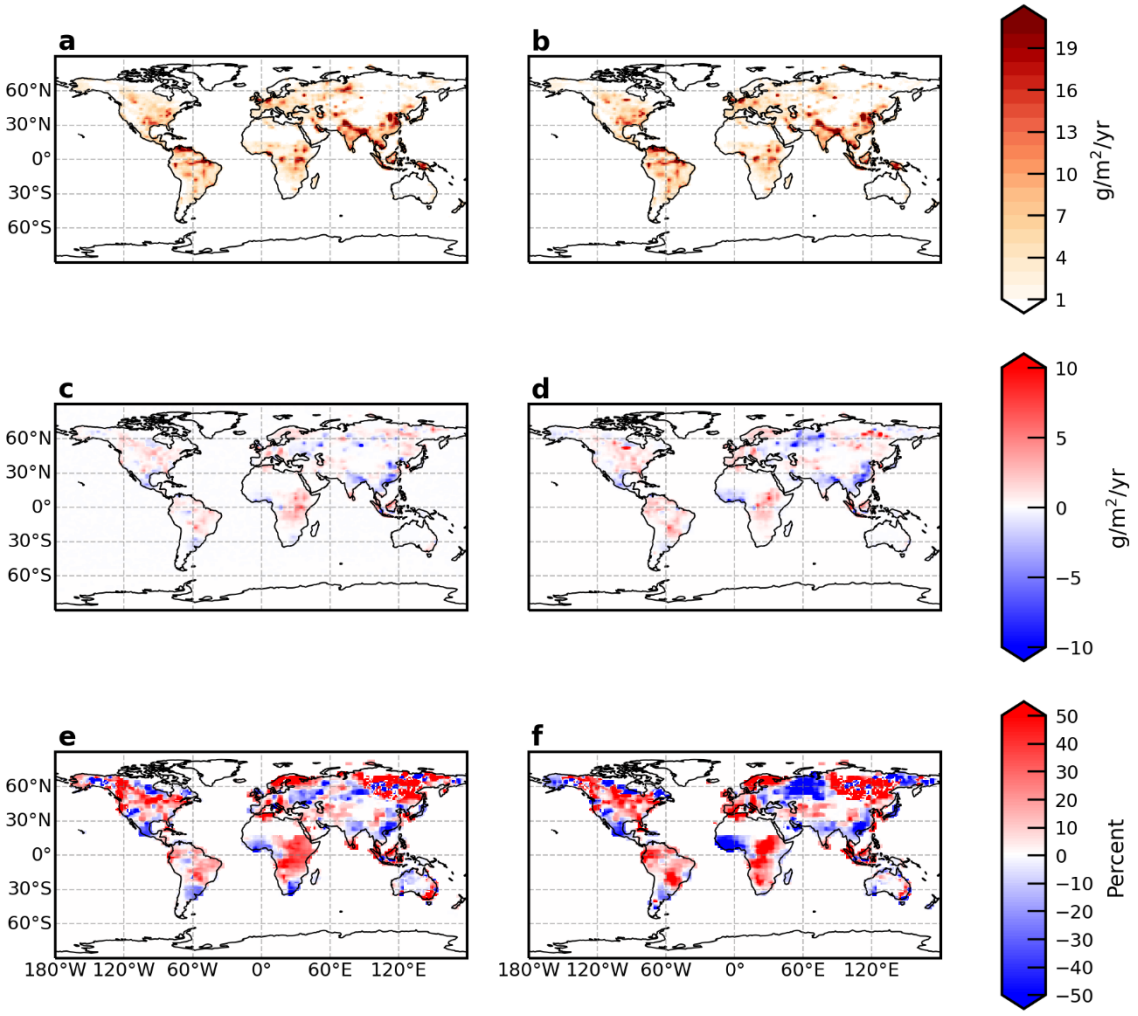

Figure 2 Global *a posteriori* emissions of methane (g/m^2/yr) inferred from GOSAT methane:CO_2 column ratio data for 2020 (panel a) and 2021 (panel b) and how they differ from the baseline year of 2019, described in terms of absolute (panels c and d, respectively) and percentage values (panels e and f, respectively).

530

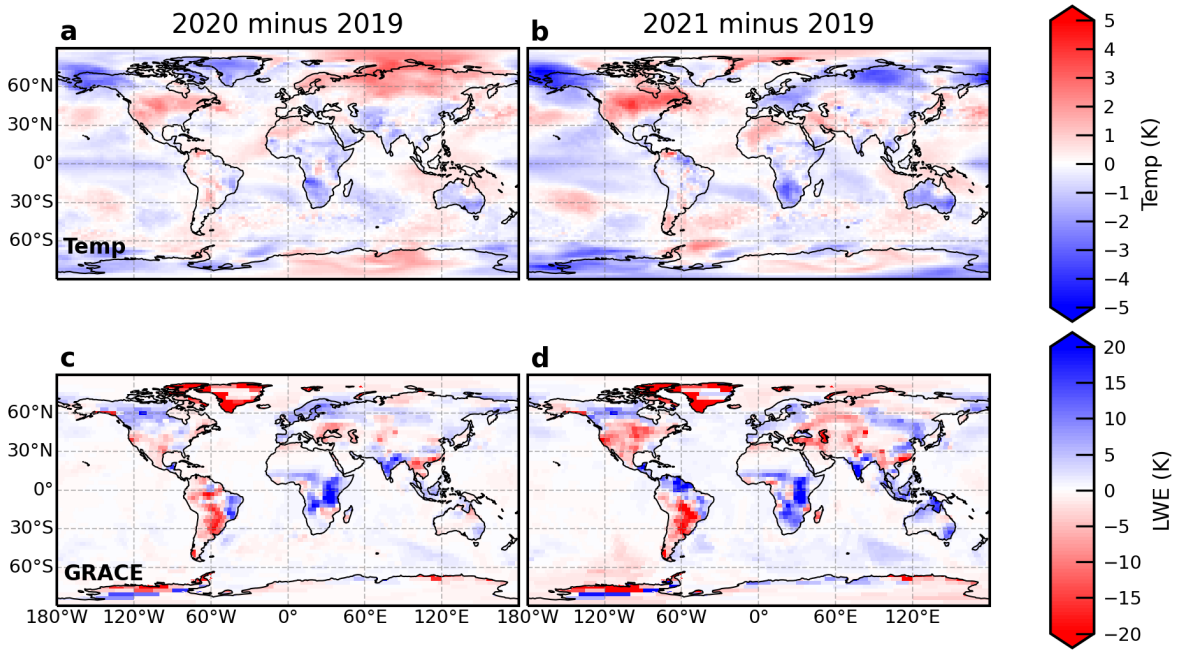

Figure 3 Global annual mean surface temperature and GRACE liquid water equivalent (LWE) anomalies in 2020 (panel a and c) and 2021 (panels b and d) relative to values in 2019.

535

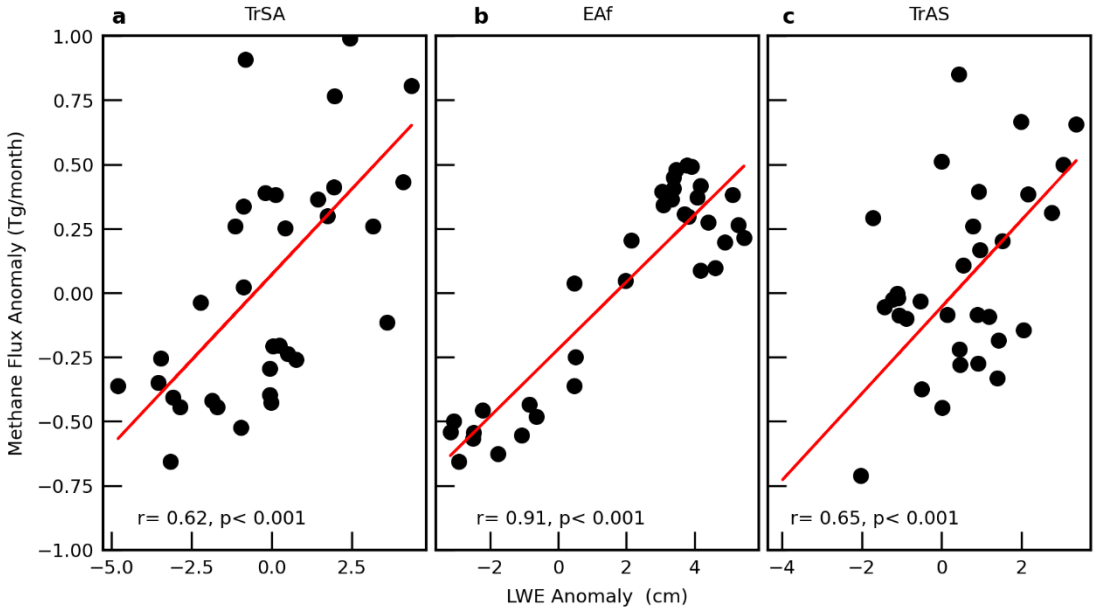

Figure 4 Scatter plot of monthly GRACE-FP LWE anomalies (cm) and methane flux anomalies, 2018-2021, over a) Tropical South America, b) Eastern Africa, and c) Tropical Asia. Red lines denote the linear regression. Numbers atop of each panel denote the Pearson correlation coefficient *r* and the p-value.

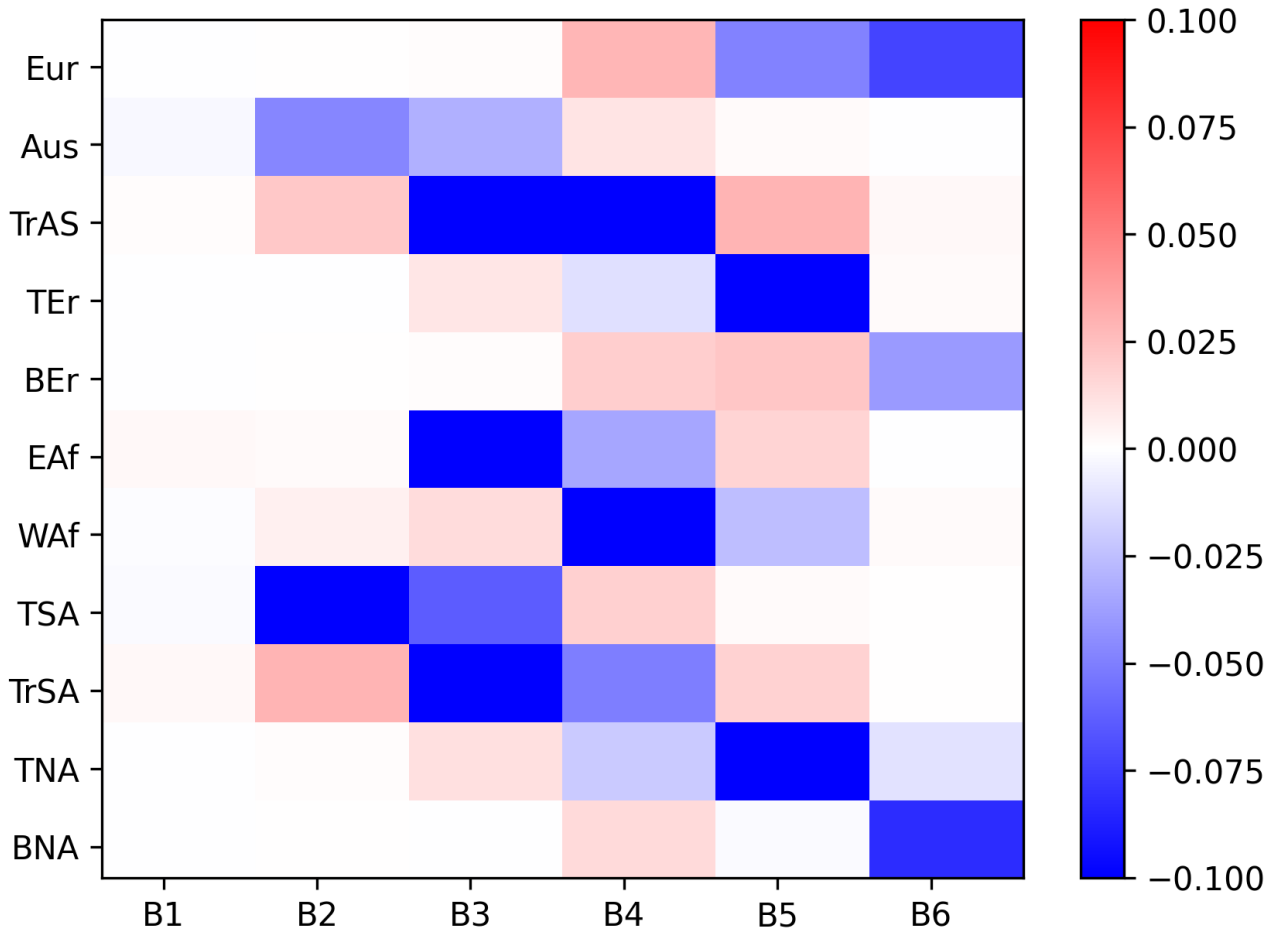

Figure 5: *A posteriori* error correlation between OH scaling factors for six latitude bands (75°S—50°S, 50°S—25°S, 25°S—0°, 0°—25°N, 25°N—50°N, 50°N—75°N) and emissions for 13 regions (Figure 1).

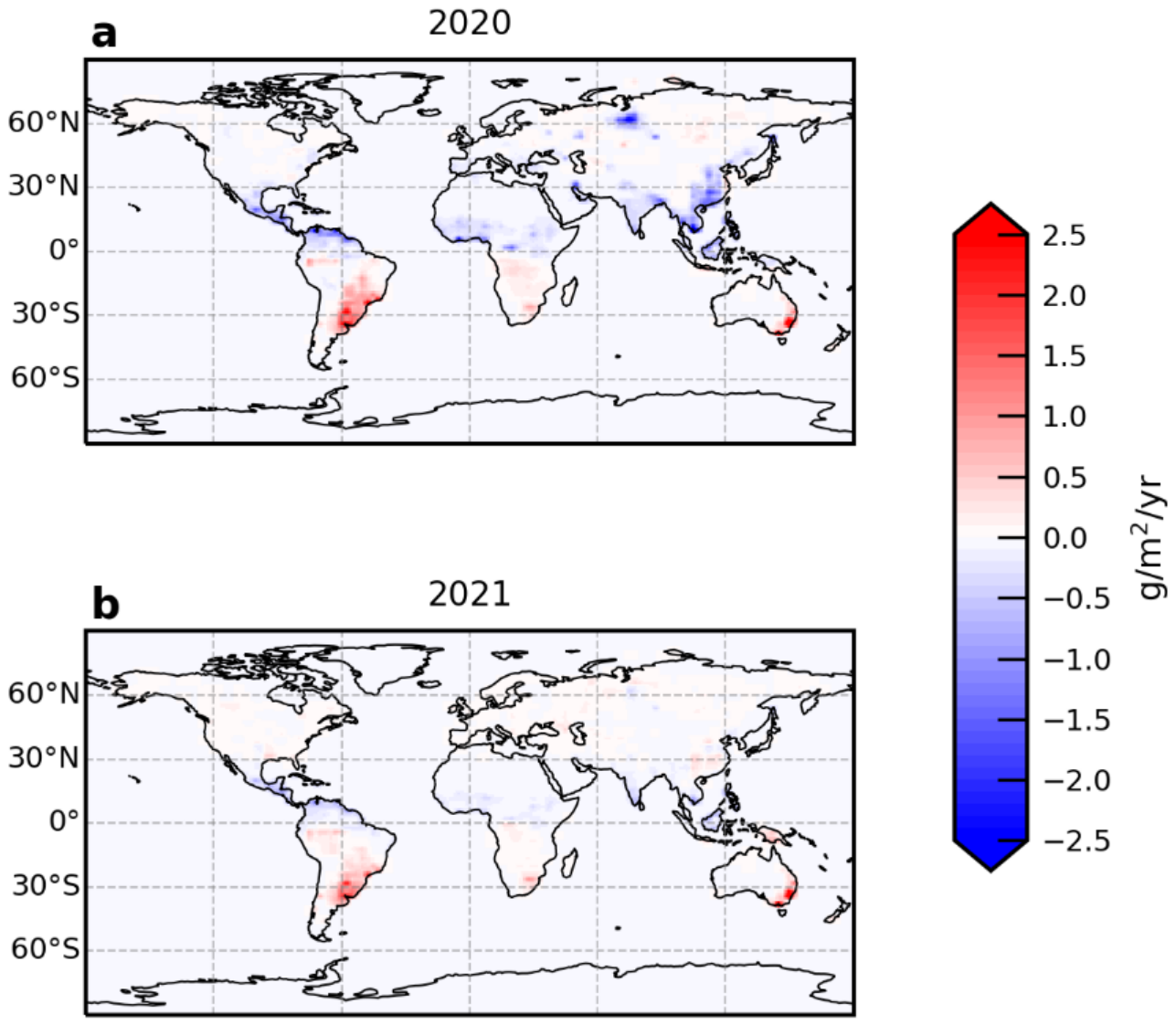

Figure 6: Annual mean difference of *a posteriori* methane emissions between the control inversion that uses OH climatology and the joint OH-Flux inversion that estimates OH scaling factors for **a** 2020 and **b** 2021.

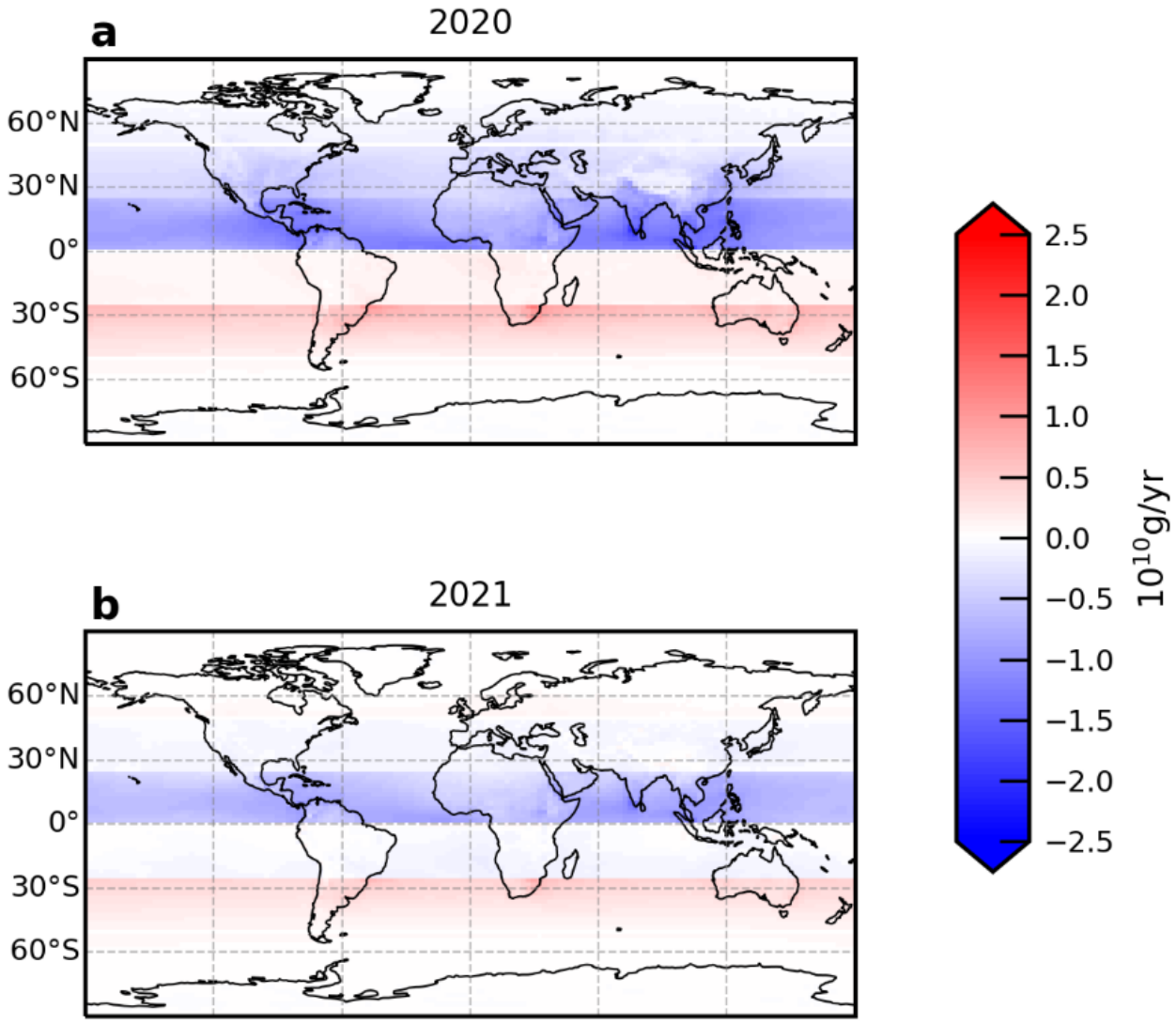

Figure 7: Annual mean difference of *a posteriori* methane loss due to OH oxidation (2020-2021) between the control inversion that uses OH climatology and the joint OH-Flux inversion that estimates OH scaling factors.

555

Tables

	Global annual methane emissions (Tg/yr)		
	2019	**2020**	**2021**
GOSAT methane inversion	583.7±11.2	610.7±11.3	604.5±11.4
GOSAT methane-OH inversion	585.3±13.1	603.2±13.2	603.7±13.2
Corresponding OH change (%)	+0.91±1.7%	-0.52±1.7%	+0.62±1.7%
In situ	588.9±18.1	601.4±18.6	--
NOAA atmospheric growth rate (ppb/yr)	9.67±0.60	15.19±0.41	18.12±0.47

Table 1 Global annual emission estimates of methane (Tg/yr) inferred from GOSAT (2019-2021) and *in situ* (2019-2020) atmospheric measurements of methane. The annual atmospheric methane growth rate (ppb/yr) for 2019 to 2022 reported by NOAA is also shown.

Experiment	OH Field	2019-2020 emission increase (Tg/yr) [% difference from control]
Control Run	Fixed OH climatology	27.0±7.1 [--]
5% OH reduction	Reduction of 5% OH over regions with high fossil CO_2 emission	20.9±7.1 [-22.6]
Ozone-like OH reduction	OH reduction following observed ozone change (Ziemke et al. 2022)	19.6±7.1 [-27.4]
Joint methane-OH inversion	18 OH scaling factors for *a priori* monthly 3-D OH fields inferred from atmospheric methane observations	20.5±7.3 [-24.1]

Table 2: Numerical experiments that explore the influence of assumed OH distributions on *a posteriori* methane emission estimates.

565

Appendix A: Supplementary Figures

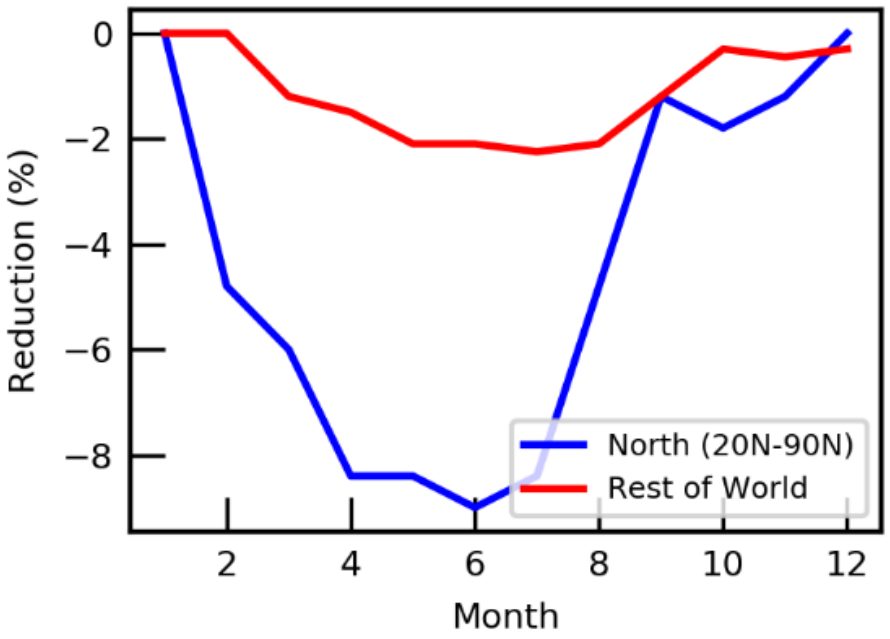

Figure A1 Assumed temporal distribution for OH reduction (%) in the northern hemisphere (20°N-90°N, blue line) and the rest of the world (red line) for our sensitivity calculation.

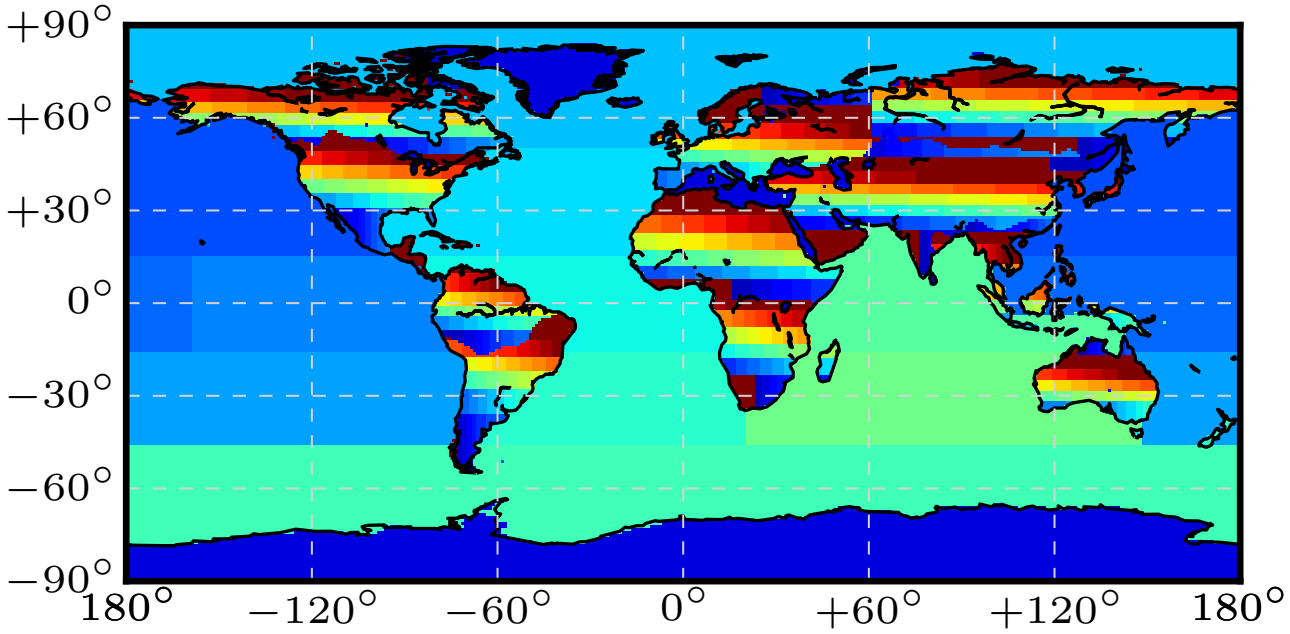

Figure A2 Basis functions that describe the 487 regions where we estimate methane emissions, including 476 land regions and 11 oceanic regions.

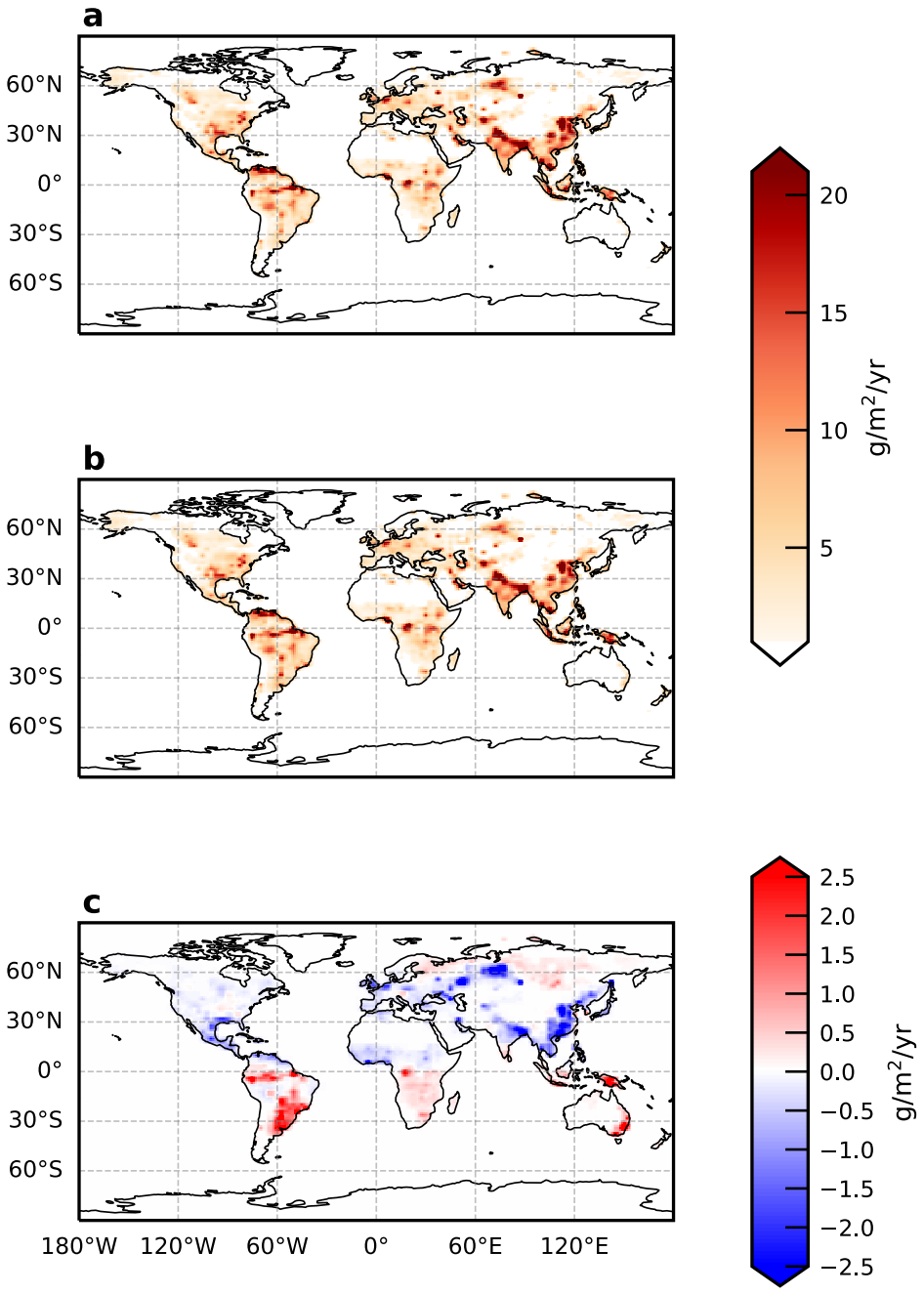

575 **Figure A3** Global *a posteriori* emissions of methane (g/m^2/yr) inferred from GOSAT methane:CO_2 column ratio data for the baseline year of 2019, corresponding to **a** OH climatology (Feng, Palmer, Zhu, et al. 2022) and **b** the joint methane-OH inversion. Panel c shows the difference of *a posteriori* emissions of methane corresponding to joint methane-OH inversion minus OH climatology.

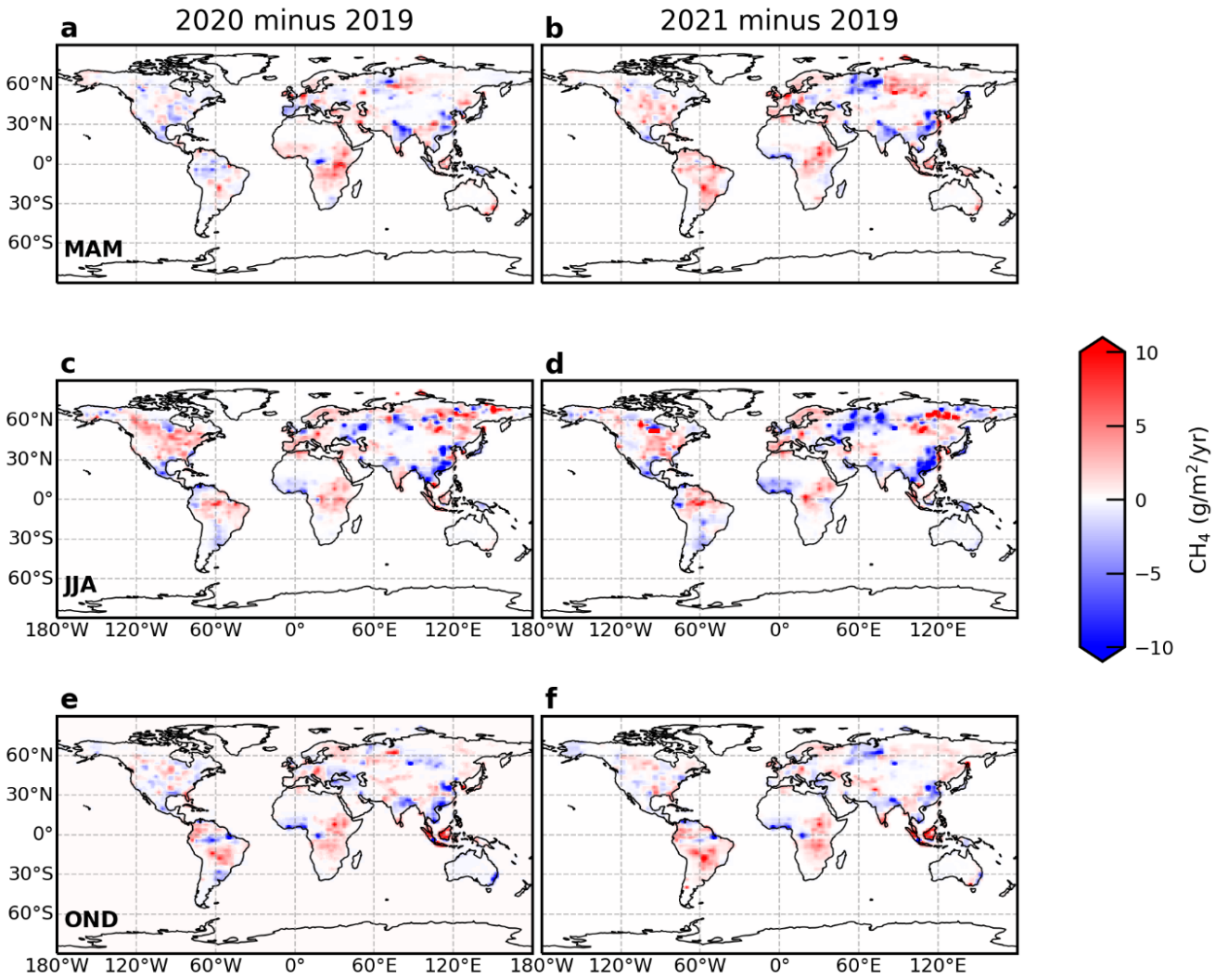

580 **Figure A4** Global seasonal *a posteriori* emissions of methane ($g/m^2/yr$) inferred from GOSAT methane:CO_2 column ratio data for 2020 (l.h.s. panels) and 2021 (r.h.s. panels) relative to the baseline year of 2019, described in terms of absolute values. Seasons are based on rainfall changes over the tropics.

585

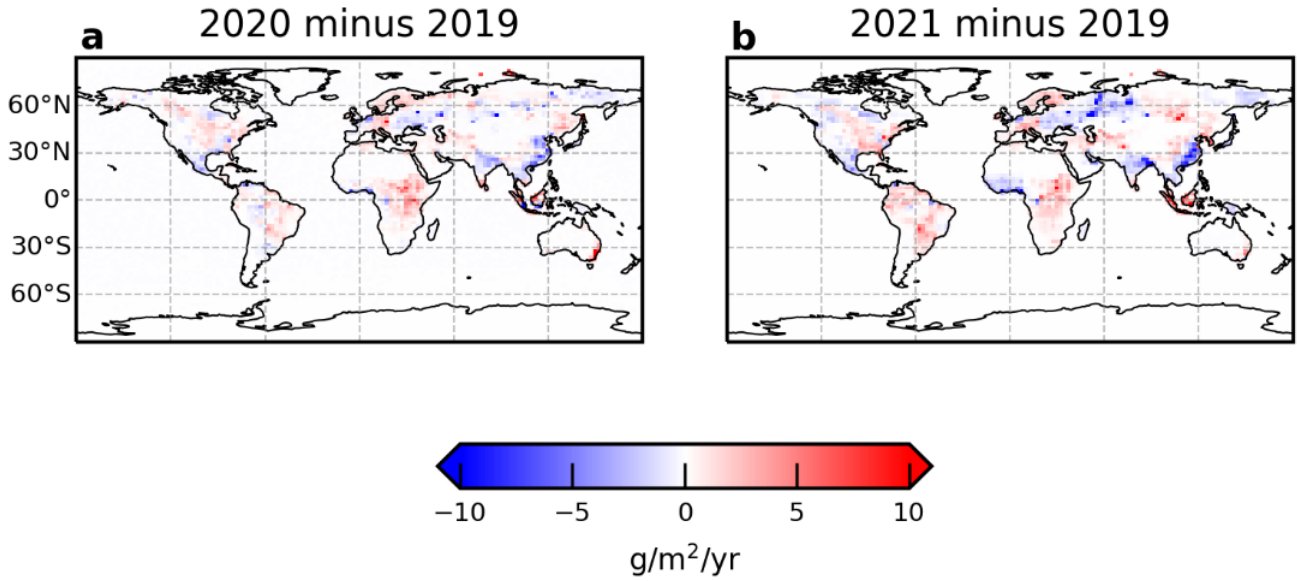

Figure A5 Global *a posteriori* emissions of methane (g/m^2/yr) inferred from GOSAT methane column data for 2020 (panel a) and 2021 (panel b).

590

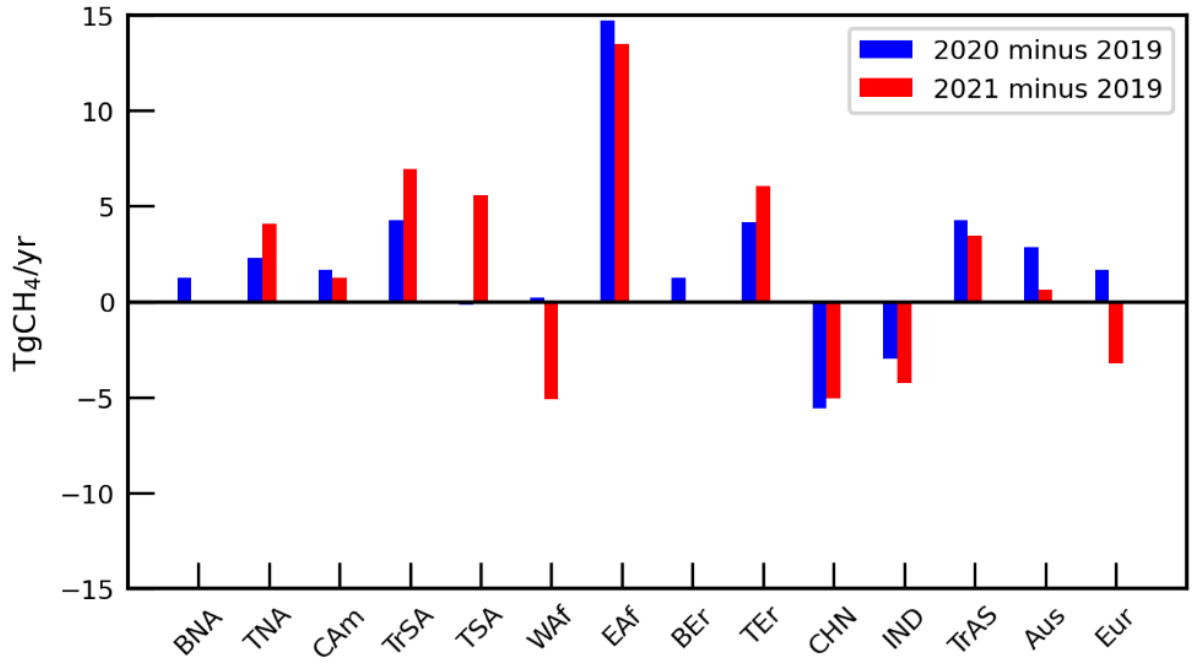

Figure A6 As Figure 1b but for an inversion that uses GOSAT proxy XCH_4 and *in situ* methane data.

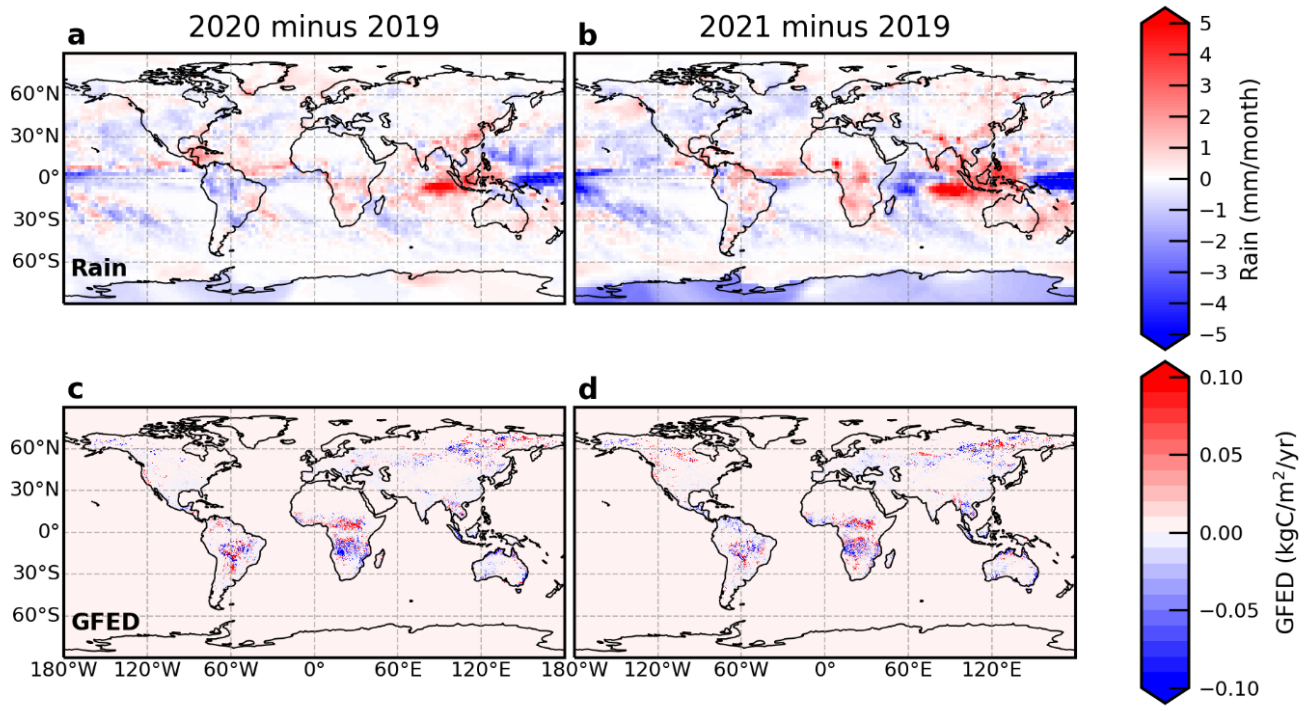

595

Figure A7 Global annual mean NOAA CMAP precipitation (mm/month/yr) and GFED fire emission (kgC/m^2/yr) anomalies in 2020 (panel a and c) and 2021 (panels b and d) relative to values in 2019.

Appendix B: Description of box model calculation

To calculate global emissions of methane from the NOAA global mean data we use a simple one-box model. In this model, the change in global mean methane concentration over time is given by:

$$\frac{dB}{dt} = Q - kB$$

where B is the atmospheric mass of methane in Tg, k is the loss rate given as 1/lifetime and Q is the emissions rate. From this, after integration, the annual emissions rate can be calculated as:

$$Q_t = \frac{k(B_t - B_{t-1} \cdot e^{-k})}{(1 - e^{-k})}$$

The loss rate was tuned to match a steady state concentration of 1775 ppb during 2000-2006 based on constant emissions of 530 Tg yr^{-1} during this period. We calculated the rolling 12-month annual emissions to track the progression of global emissions between 2019 and 2021. We used the difference between the atmospheric concentration in January 2019 and January 2020, February 2019 to February 2020, etc. to calculate the change in emissions in the intervening 12 months. Figure B1 shows the increase in emissions throughout 2020 followed by more variable month-to-month changes in 2021. The large increase in emissions primarily occurs in 2020, with emissions at the 12-month period ending in Dec 2020 being 27 Tg yr^{-1} larger than the emissions one year earlier. In contrast if emissions are calculated using annual mean concentrations, it appears as if there is a larger emission increase in 2021. The box model results show that the highly simplified calculation based on global average data is consistent with the more complex inverse modelling approach applied to the GOSAT data.

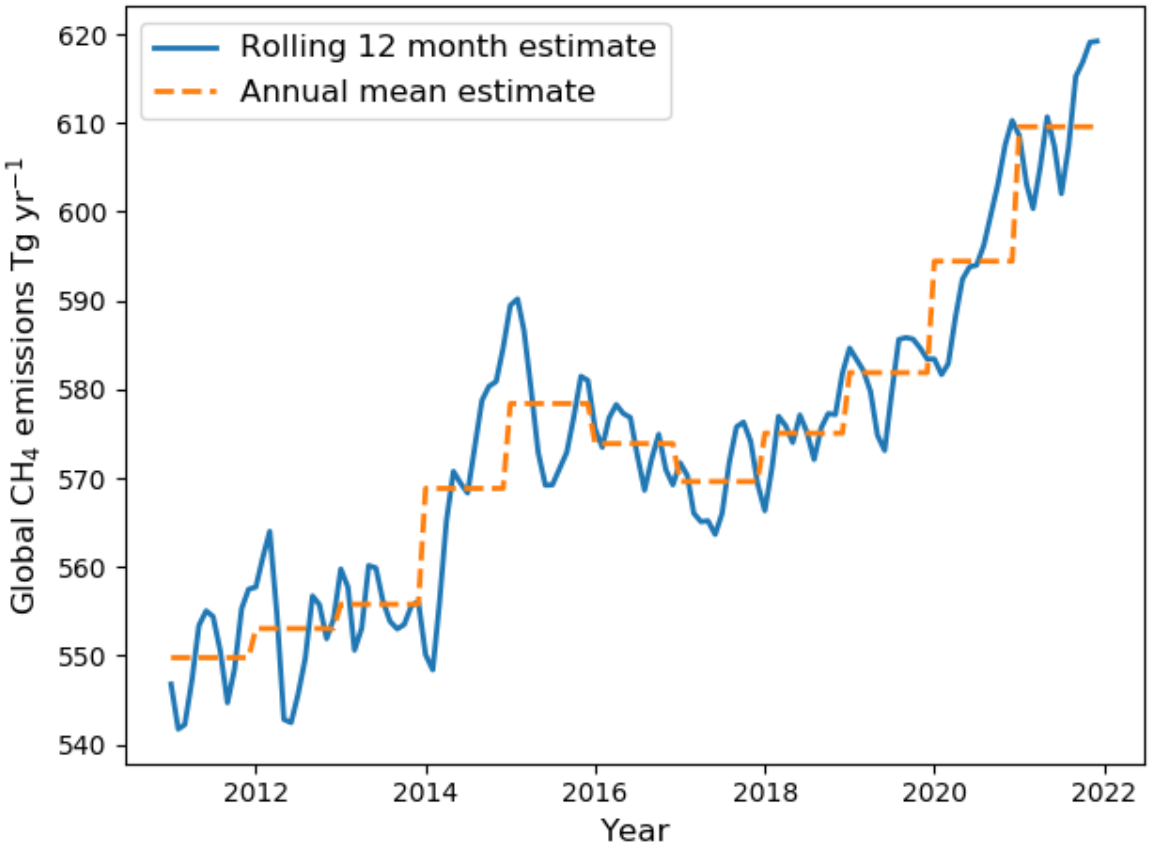

Figure B1 Global box model methane emission estimates between 2011 and 2021, respectively. Emission estimates are based on NOAA global mean surface data. The blue line denotes the rolling 12-month annual emissions, and the orange line denotes the emissions based on annual mean concentrations.

Appendix C: Evaluation of *a posteriori* flux estimates

We indirectly evaluate our *a posteriori* methane fluxes by comparing the GEOS-Chem methane distribution, driven by the *a posteriori* fluxes, with independent XCH_4 retrievals from Total Carbon Column Observing Network (TCCON) of Fourier transform spectrometers (Wunch et al., 2011). We use bias-corrected TCCON XCH_4 data from the latest GGG2020 public release of the TCCON data set from 2019 to 2021, including updates until October 2022. For a comprehensive description of the network and the available data from each TCCON site, we refer the reader to the TCCON project page. Here we use a subset of available TCCON data, dependent on their availability between 2018 and 2021 (Buschmann et al. 2022; De Mazière et al. 2022; García et al. 2022; Hase et al. 2022; Kivi, Heikkinen, and Kyrö 2022; Liu et al. 2022; Morino, Ohyama, et al. 2022b; Morino, Velazco, et al. 2022; Morino, Ohyama, et al. 2022a; Notholt et al. 2022; Petri et al. 2022; Pollard, Robinson, and Shiona 2022; Warneke et al. 2022; Shiomi et al. 2022; Té, Jeseck, and Janssen 2022; Wennberg, Wunch, et al. 2022; Wennberg, Roehl, Wunch, Blavier, et al. 2022; Wennberg, Roehl, Wunch, Toon, et al. 2022; Wunch et al. 2022; Zhou et al. 2022). For further details about the data we direct the reader to the TCCON project page: http://tccondata.org/.

Figure C1 shows the mean and standard deviation of the differences between our *a posteriori* model simulation and TCCON GGG2020 data in 2019 and 2020. The *a posteriori* model simulation is driven by our *a posteriori* methane emission estimates. We sample the associated model 3-D atmospheric methane distributions at the time and location of each TCCON site used. We then convolve the sampled vertical profile with site- and time-dependent TCCON instrument averaging kernels, which describes the altitude-dependent instrument sensitivity to changes in atmospheric methane concentration. Figure C2 shows the same statistical comparison but using the *a posteriori* methane emission estimates inferred with the OH scaling factors, as described in section 2.4.

We do not report results for 2021 due to data availability; for data that are available, we find the mean statistics (not shown) are similar to those we report here for 2019 and 2020. For most sites, we find the mean bias is typically smaller than ±10 ppb and the standard deviation has a range 5-15 ppb with typically values smaller than 10 ppb. We find the largest differences at northern high latitudes where the model has a large overestimate (~10 ppb), consistent with previous studies (Feng et al., 2017, 2022), due to poor coverage of GOSAT data during the boreal winter and to model error.

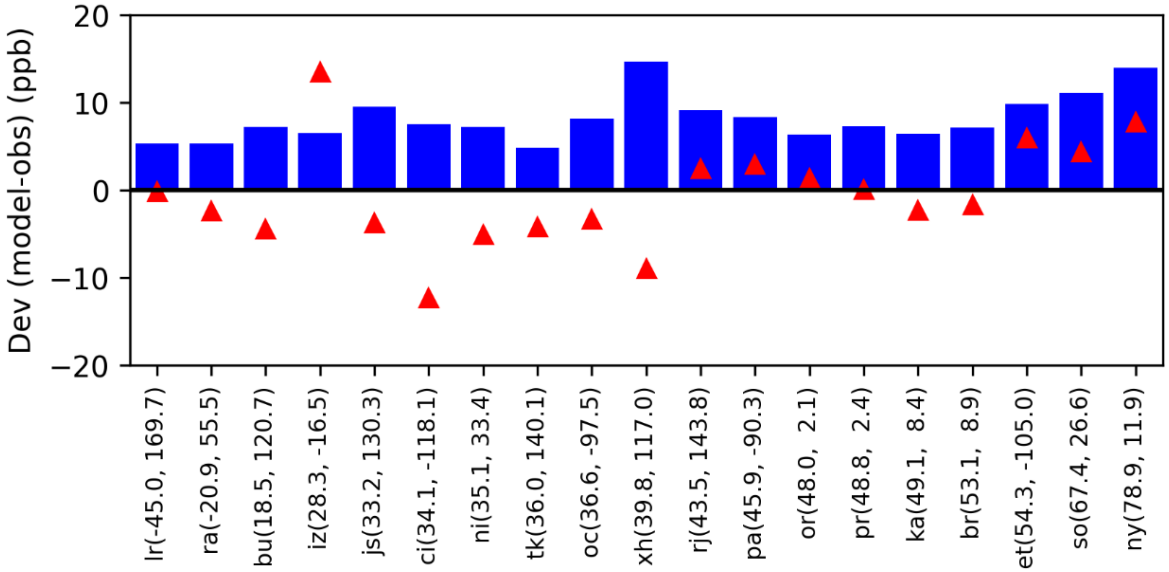

Figure C1 Statistical comparison of the GEOS-Chem *a posteriori* methane distribution and TCCON XCH_4 data (v GGG2020) in 2019 and 2020. Red upward triangles denote the mean bias and the blue bars denote the corresponding 1s values.

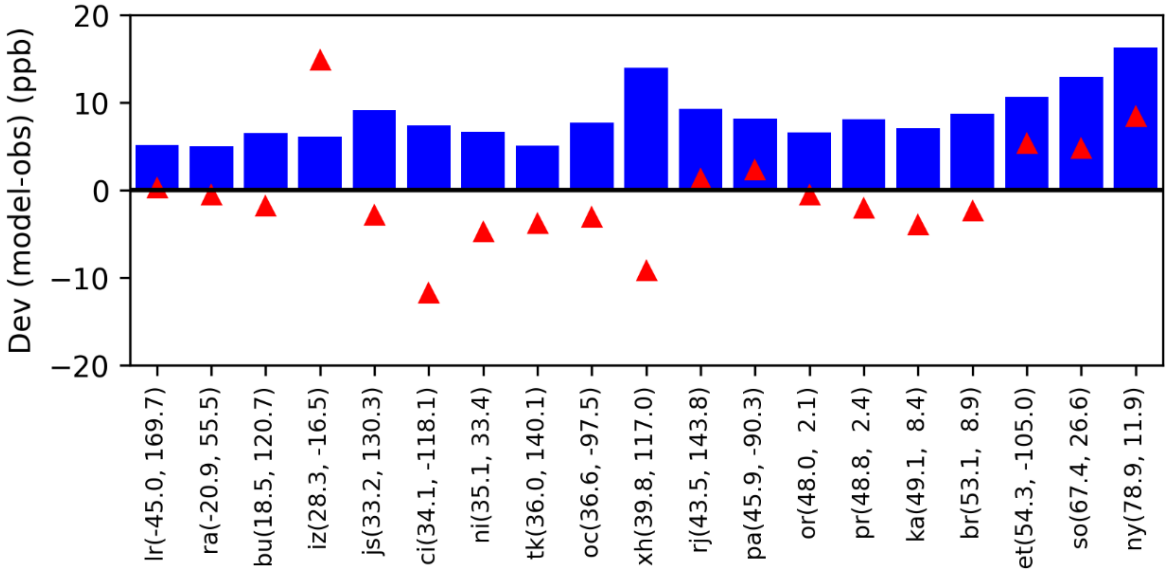

Figure C2 The same as Figure C1 but for the inversion that also includes OH scaling factors.